AGU PUBLICATIONS

Water Resources Research

RESEARCH ARTICLE
10.1002/2017WR021240

Key Points:
- The study provides a methodology to assess the potential geochemical impacts of large-scale water injection
- Reactive transport modeling was used to incorporate field and laboratory experimental data to understand arsenic mobilization processes
- A new Monte Carlo framework was developed to efficiently quantify the predictive uncertainty of the long-term fate of arsenic

Correspondence to:
H. Prommer,
henning.prommer@csiro.au

Citation:
Rathi, B., Siade, A. J., Donn, M. J., Helm, L., Morris, R., Davis, J. A., . . . Prommer, H. (2017). Multiscale Characterization and Quantification of Arsenic Mobilization and Attenuation During Injection of Treated Coal Seam Gas Coproduced Water into Deep Aquifers. *Water Resources Research*, *53*, 10,779–10,801. https://doi.org/10.1002/2017WR021240

Received 1 JUN 2017
Accepted 30 NOV 2017
Accepted article online 4 DEC 2017
Published online 26 DEC 2017

Multiscale Characterization and Quantification of Arsenic Mobilization and Attenuation During Injection of Treated Coal Seam Gas Coproduced Water into Deep Aquifers

Bhasker Rathi[1,2], Adam J. Siade[1,2,3], Michael J. Donn[3], Lauren Helm[4], Ryan Morris[4], James A. Davis[5], Michael Berg[6], and Henning Prommer[1,2,3]

[1]School of Earth Sciences, University of Western Australia, Nedlands, WA, Australia, [2]CSIRO Land and Water, Australia, Private Bag No. 5, Wembley, WA, Australia, [3]National Centre for Groundwater Research and Training (NCGRT), Bedford Park, SA, Australia, [4]Origin Energy, 339 Coronation Drive, Milton, QLD, Australia, [5]Lawrence Berkeley National Laboratory, Earth Sciences Division, Berkeley, CA, USA, [6]Eawag, Swiss Federal Institute of Aquatic Science and Technology, Düben dorf, Switzerland

Abstract Coal seam gas production involves generation and management of large amounts of co-produced water. One of the most suitable methods of management is injection into deep aquifers. Field injection trials may be used to support the predictions of anticipated hydrological and geochemical impacts of injection. The present work employs reactive transport modeling (RTM) for a comprehensive analysis of data collected from a trial where arsenic mobilization was observed. Arsenic sorption behavior was studied through laboratory experiments, accompanied by the development of a surface complexation model (SCM). A field-scale RTM that incorporated the laboratory-derived SCM was used to simulate the data collected during the field injection trial and then to predict the long-term fate of arsenic. We propose a new practical procedure which integrates laboratory and field-scale models using a Monte Carlo type uncertainty analysis and alleviates a significant proportion of the computational effort required for predictive uncertainty quantification. The results illustrate that both arsenic desorption under alkaline conditions and pyrite oxidation have likely contributed to the arsenic mobilization that was observed during the field trial. The predictive simulations show that arsenic concentrations would likely remain very low if the potential for pyrite oxidation is minimized through complete deoxygenation of the injectant. The proposed modeling and predictive uncertainty quantification method can be implemented for a wide range of groundwater studies that investigate the risks of metal(loid) or radionuclide contamination.

1. Introduction

Coal seam gas (CSG) has become an important source of energy around the world in just over 30 years of its commercial production (Clarkson & Bustin, 2011). USA and Australia are currently the main producers, with Canada, China, India and various other countries planning to increase their investments in the CSG industry. Production of CSG is achieved by reducing the groundwater pressure within the coal seams, which releases methane from the coal in the form of gas. While methane is extracted, it is accompanied by large volumes of co-produced water (Schraufnagel, 1993). Current projections indicate that the Australian CSG industry alone will extract on the order of 3,200 gigaliters (GL) of water from groundwater systems over the next 45 years, with an average production of 70 GL per year (GL/yr) (DNRM, 2016). Management of large volumes of co-produced water is a potential concern due to the elevated water salinity and the presence of residual organic substances. This water is managed in different ways at different locations with the primary methods being disposal to surface waters and water reuse (Hamawand et al., 2013). Most of the CSG production sites in Australia are based in the semi-arid regions of New South Wales and Queensland where the release of large volumes of co-produced water into surface water systems could alter both natural flow and hydrochemical patterns, resulting in potentially significant ecological impacts. Therefore at these sites, the injection of co-produced water into deeper aquifers after a comprehensive treatment process is seen as the most viable and socially acceptable option, besides providing treated water for irrigation purposes.

The site-specific technical and economic feasibility of large-scale CSG water injection depends on a combination of operational, hydrogeological and geochemical factors. Understanding the geochemical response to the injection of CSG waters and the underlying mechanisms is important for predicting the long-term groundwater quality evolution, and to prevent any undesired deterioration of the groundwater quality. However, due to the often significant depth of the injection targets, significant costs of setting up infrastructure for an injection scheme, and the economic pressures of CSG production, the target aquifers generally do not undergo detailed characterization either geochemically or mineralogically.

One of the most concerning geochemical risks to receiving aquifers is the potential for arsenic mobilization from aquifer sediments (Neil et al., 2012). The release of arsenic has been observed at numerous managed aquifer recharge sites around the world due to several different geochemical mechanisms. For example, the injection of aerobic water can induce pyrite oxidation and subsequently, the release of arsenic incorporated within the mineralogical structure (Wallis et al., 2010, 2011). Furthermore, McNab et al. (2009) showed that the elevated pH of the recharged water induced desorption of arsenic at a managed aquifer recharge site in California's San Joaquin Valley. Also, Appelo and Vet (2003) and later Vanderzalm et al. (2011) reported cases where elevated phosphate levels in the injectant caused the mobilization of arsenic through competitive desorption.

The most valuable information for predicting geochemical impacts, including the risk of metal(loid) mobilization by large-scale injection schemes can often be obtained from monitoring of short-term injection trials (Seibert et al., 2016). The hydrochemical data collected during such trials can be analyzed and integrated with any additionally available information from pre-trial geochemical characterization efforts and supporting laboratory experiments, such as batch sorption experiments. For example, the data obtained from laboratory batch sorption experiments for metals or metalloids can be analyzed through geochemical models that incorporate a surface complexation model (SCM). Subsequently, the SCM developed for the laboratory-scale may be incorporated into the field-scale model and used for process-based predictions of the long-term geochemical behavior through the application of reactive transport models (RTM). For example, Kent et al. (2000) employed a semi-empirical SCM that was developed from laboratory experimental data to simulate zinc transport at the Cape Cod field site. Similarly, Curtis et al. (2006) investigated uranium transport in a shallow alluvial aquifer beneath a former mill located near Naturita, CO, by using their laboratory-derived SCM to describe U(VI) adsorption in a field-scale RTM. Also, Ma et al. (2014) used the SCM developed by Stoliker et al. (2011) to simulate the field-scale uranium transport processes at the Hanford 300A site under highly transient flow conditions.

However, there are a number of challenges associated with this type of integrated, multi-scale modeling approach. Natural aquifer sediments contain an assemblage of minerals and organic materials. The generalized composite approach for SCM (GC-SCM) (Davis et al., 1998) has been considered the best approach for taking into account the inherent chemical and physical heterogeneity of natural sediments. The GC-SCM is calibrated to sediment-based sorption data and its parameters are estimated by inverse modeling. Although the resulting GC-SCMs are generally nonlinear and their parameters can be estimated more effectively using heuristic algorithms (Rathi et al., 2017), such as particle swarm optimization (PSO) (Eberhart & Kennedy, 1995), there is an underlying uncertainty associated with these parameters. The quantification of this uncertainty is often computationally infeasible for field-scale RTMs. When upscaling a SCM from the laboratory-scale to a field-scale RTM, the differences in heterogeneity, i.e., the size and mass of the two systems can play a significant role and must be accounted for. However, the effects of parameter uncertainty in the laboratory SCM and on field-scale simulations have not been examined. We hypothesize that parameter uncertainty can lead to significant predictive uncertainty when using a field-scale RTM to assess long-term geochemical behavior. There have been some studies that have addressed computational considerations for predictive uncertainty using simple RTMs. For example, Tartakovsky et al (2009) use sophisticated probability density function (pdf) techniques, resulting in reduced computational effort, to explore uncertainty associated with reactive solute concentrations for a simple, single-reaction, single-species synthetic case study. However, there is currently no study addressing the complex multi-species, multi-reaction GC-SCM and its associated impacts on predictive uncertainty in a real-world setting. Due to the complexity and numerical requirements associated with GC-SCMs, it is likely that Monte Carlo methods are the most viable for quantifying predictive uncertainty associated with these models. However, since the CPU run-times of GC-SCMs are very fast, Monte Carlo procedures can be quite effective, and their associated results can be up-scaled to the field-scale RTM.

In this study, we explore the integration of laboratory-scale data and models into the analysis of a CSG water injection experiment at the field-scale. We propose a new practical procedure for upscaling laboratory-derived GC-SCM parameters to be used in a field-scale RTM for the subsequent quantification of parametric and predictive uncertainty. Our approach alleviates a significant proportion of the computational effort required for predictive uncertainty quantification when using field-scale RTMs within a Monte Carlo framework. This is accomplished by exploiting the extremely fast execution time associated with laboratory based GC-SCMs. We use this framework to identify and characterize the mobilization and attenuation mechanisms that control the risk of generating elevated arsenic concentrations in response to large-scale, long-term (re-)injection into deep aquifers.

2. Field Injection Study

2.1. Field Site

The site that provided the data and motivation for this study is located approximately 70 km northeast of Roma in the southeast of Queensland, Australia. It is situated in the Surat Basin, a sub-basin of the Great Artesian Basin. The CSG and co-produced water are produced from the Jurassic age Walloon Coal Measures between 450 – 800 m below ground surface (BGS). The co-produced water was treated via reverse osmosis (RO) and de-oxygenated prior to reinjection into the Precipice Sandstone formation (>1,300 mBGS). The lowermost portion of this formation is known as the Braided Stream Facies (BSF), which is the most permeable zone of the overall formation, composed of relatively coarse-grained material representative of a high-energy fluvial depositional environment (Green et al., 1997).

2.2. Geochemical and Geophysical Characterization

The Precipice formation is characterized by quartzose sandstone, which is fine-textured in the upper portions of the formation and becomes more coarse-textured with depth (Exon, 1976). Aquifer material from the Braided Stream Facies sub-unit of the Precipice Sandstone aquifer, collected at various depths from 1300.87 to 1346.50 mBGS, was used for sediment characterization via laboratory experiments. Mineralogical analysis of this aquifer material using quantitative X-ray diffraction (XRD) identified quartz to be the dominant mineral with up to 5% of clay minerals (kaolinite and illite), while crystalline iron minerals, such as goethite, hematite and pyrite, and carbonate minerals were not detected. The major components identified by elemental analysis (XRF) were SiO_2 (96.45 wt%), Al_2O_3 (1.93 wt%) and K_2O (0.17 wt%) reflecting the dominance of quartz, clay and feldspar minerals, while total Iron, as Fe_2O_3, was present in a minor quantity of 0.15 wt%. The XRD and XRF analyses were carried out at the CSIRO Mineralogical and Geochemical Services Centre (Urrbrae, SA).

Wireline geophysical logging of the injection target was undertaken prior to running screens. The screened interval was 1285.4–1376.5 mBGS and included the upper Precipice Sandstone, the BSF and 30 m of the underlying Moolayember Formation, a shale. The BSF had a gross thickness of 21.2 m. A gamma response of less than 40GAPI suggested a net sand interval of 19.7 m. Porosity values measured using the neutron density method ranged from 2% in the Moolayember Formation to up to 30% in the BSF. Formation Micro-imager (FMI) logs did not identify any fracturing through the BSF. However, fracturing was observed in the underlying Moolayember Formation. Core samples show many of these fractures to be polished into a glass.

2.3. Field Injection Trial

Due to the large depth of the target aquifer and associated costs of installing monitoring bores, the injection trial was undertaken as a push-pull test in which a single well was used for injection into, and extraction from, the targeted aquifer. A total of 52.7 megaliters (ML) of treated co-produced water was injected for 65 days spread over an 85 days period, followed by a storage period of 64 days to allow the injected water to react with the native groundwater and the aquifer matrix. Finally, a recovery phase was operated for a total of 309 days and 156 ML of water was extracted, representing approximately three times the total water injected. Samples of the injected water were collected for laboratory analysis weekly for the first month, then fortnightly until the end of injection phase. During the recovery phase, water quality samples were collected twice per day for a period of two weeks, then on a weekly basis until the majority of the injected water was recovered, followed by intermittent sampling. A bromide tracer amendment was undertaken

Table 1
Summary of Hydrochemical Compositions

		Injectant		Recovered	
Analyte	Background	Avg.	Max.	Avg.	Max.
Na (mol/L)	7.74×10^{-3}	4.05×10^{-3}	7.05×10^{-3}	6.57×10^{-3}	7.66×10^{-3}
Cl (mol/L)	2.80×10^{-3}	2.06×10^{-3}	4.34×10^{-3}	3.53×10^{-3}	4.20×10^{-3}
HCO_3 (mol/L)	2.59×10^{-3}	9.70×10^{-4}	1.06×10^{-3}	1.43×10^{-3}	2.89×10^{-3}
pH	7.80	9.34	9.4	8.5	8.9
Temperature (°C)	62	18	26	41	50
Si (mol/L)	5.44×10^{-4}	2.55×10^{-5}	4.16×10^{-5}	3.33×10^{-4}	5.29×10^{-4}
SO_4 (mol/L)	$< 1.04 \times 10^{-5}$	$< 1.04 \times 10^{-5}$	$< 1.04 \times 10^{-5}$	3.12×10^{-5}	4.16×10^{-5}
Reactive P (mol/L)	6.60×10^{-6}	$< 3.23 \times 10^{-7}$	$< 3.23 \times 10^{-7}$	1.94×10^{-6}	3.23×10^{-6}
As (mol/L)	1.60×10^{-8}	$< 1.33 \times 10^{-8}$	$< 1.33 \times 10^{-8}$	2.27×10^{-7}	3.20×10^{-7}
Dissolved Oxygen (mol/L)	Not measured	$< 1.25 \times 10^{-5}$	1.25×10^{-5}	Not measured	Not measured

toward the end of the injection phase. No additional bores were available on-site to monitor the water quality within the radius of influence of the injection bore.

2.4. Background Water Composition

Groundwater in the Precipice Sandstone formation at the study site prior to commencement of the injection experiment was highly reducing containing 4.67×10^{-4} mol/L dissolved methane and strongly dominated by sodium (7.74×10^{-3} mol/L), while chloride was the most dominant anion (2.80×10^{-3} mol/L) followed by bicarbonate (2.59×10^{-3} mol/L). Calcium concentrations were below the detection limit (2.45×10^{-5} mol/L). Field pH and temperature measurements averaged to 7.86 and 62°C, respectively. Average background alkalinity was 2.59×10^{-3} mol/L while the concentrations of silica and reactive phosphorus were 5.44×10^{-4} mol/L and 3.29×10^{-6} mol/L, respectively. Sulfate and arsenic concentrations were found to be below the detection limit of 1.04×10^{-5} mol/L and 1.33×10^{-8} mol/L, respectively. All analytes of the background water composition are listed in Table 1.

2.5. Injectant Water

CSG co-produced water was stored in an open 120 ML lined pond prior to transfer to the treatment facility. The treatment methods for the injectant included coarse filtration of suspended solids, ultrafiltration (UF), reverse osmosis (RO), ultra-violet (UV) irradiation and deoxygenation by membrane contactors. The water quality was closely monitored during both the injection and recovery periods. Water quality parameters, such as dissolved oxygen (DO), electrical conductivity (EC), pH, redox potential (ORP) and temperature of the injectant water were recorded at a one-second interval by the process control system.

Sodium was the most dominant cation (4.05×10^{-3} mol/L) in the injectant while chloride was the most dominant anion (2.06×10^{-3} mol/L), followed by bicarbonate (9.70×10^{-4} mol/L). Calcium concentrations were below the detection limit (2.45×10^{-5} mol/L). The pH and temperature measurements in the field averaged to 9.3 and 19°C, respectively. The high pH of injected water could be attributed to degassing of CO_2 during storage in an open pond. Sulfate, reactive phosphorus and arsenic were not detected in the injectant. Low concentrations of silica (2.55×10^{-5} mol/L) were also measured (Table 1 and Figure 1).

A bromide tracer amendment was undertaken to determine the physical transport behavior at the study site. Two separate pulses of 8.00×10^{-3} mol/L of *NaBr* were injected to increase the identifiability of the observed tracer concentration in response to the complex injectant signal. The tracer amendment was carried out toward the end of the injection phase (Figure 1) to minimize the required recovery period and to prevent the excessive dilution of bromide. The tracer solution was prepared by mixing 25kg of laboratory grade *NaBr* powder into the 30,000 L blending tank and was injected over approximately 4 hours.

2.6. Observed Geochemical Response

The recovered water initially displayed a similar ionic composition to that of the injectant water, with generally no clear evidence of reactive processes. After the initial recovery phase, observed concentrations

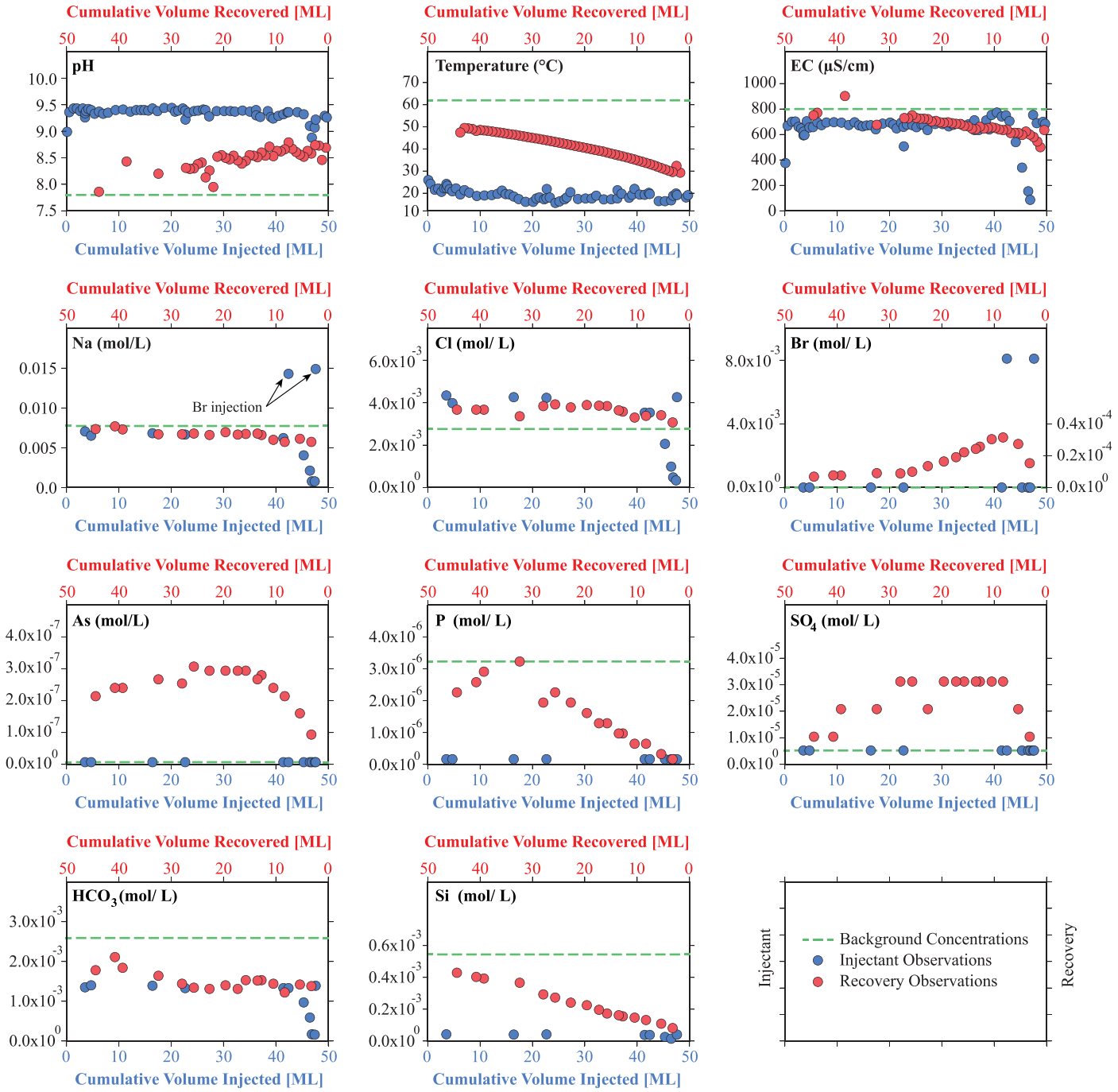

Figure 1. Field injection trial average aqueous chemical compositions. Background composition of groundwater was dominant in sodium, chloride and bicarbonate ions, had an average pH of 7.86 and had high temperatures. Arsenic concentrations were below the detection limit of 1.33×10^{-8} mol/L. Injectant composition had similar EC values and sodium, chloride, bromide, arsenic and sulfate concentrations as that of the background groundwater. However, injectant had much higher pH but lower temperature, and phosphate, bicarbonate, and silica concentrations than the background. Two pulses of bromide tracer (8.00×10^{-3} mol/L) were amended near the end of injection phase. Initial stages of recovery displayed similar ionic composition to that of the injectant followed by the effects of reactive processes such as release of arsenic (3.20 × 10-7 mol/L) and sulfate (4.16×10^{-5} mol/L). Finally, the composition of the recovered water returned to the background conditions.

showed a general trend toward background conditions (Figure 1). The field-measured pH of the recovered water showed a successive transition from 8.79 toward background conditions (7.86). Both silica and reactive phosphorus also returned to the background groundwater concentrations.

While absent in the background groundwater, sulfate was found in the recovered water at concentrations of up to 4.16×10^{-5} mol/L, indicating that mineral dissolution must have occurred, releasing sulfate during subsurface residence of the injectant. The bromide breakthrough curve was observed during the initial recovery phase producing a distinct peak of 3.75×10^{-5} mol/L (Figure 1).

The most noteworthy geochemical response occurred for arsenic, which peaked at a maximum concentration of 3.20×10^{-7} mol/L during the initial recovery phase, as arsenite (As(III) (Figure 1). This concentration of arsenic is above the World Health Organization (WHO) and Australian drinking water guideline of 1.33×10^{-7} mol/L) but far below the water quality guideline of 6.67×10^{-6} mol/L for livestock use applicable to the Precipice aquifer targeted for injection in this study (ANZECC, 2000). Among a range of possible geochemical mechanisms that have the potential to cause arsenic mobilization, arsenic desorption from sediment surfaces due the injectant being more alkaline than the receiving groundwater appeared to be the most likely. To test this hypothesis and to quantify the arsenic sorption (adsorption/desorption) capacity and characteristics, a series of laboratory sorption experiments were performed with aquifer sediments under controlled geochemical conditions.

3. Laboratory-Based Characterization of Arsenic Sorption Behavior

3.1. Arsenic Sorption Experiments

The sorption experiments were carried out with sediment samples collected at a depth of 1332.53–1333.55 mBGS. The material was sieved to a size <2.0 mm and composited anaerobically. Batch experiments were carried out using 4.00 g of sediment material combined with an electrolyte solution of 40 mL of 6 mM *NaCl*. The ionic strength of this solution was comparable to the background groundwater of the target injection zone. This solution was prepared using deionized water, which was de-oxygenated by purging with nitrogen gas for 4–5 hours and stored overnight in an anaerobic chamber (Coy Laboratories, Model AALC) containing a N_2/H_2 mixture, with 2% H_2 gas. Dissolved oxygen in this solution was not detected when measured using a WTW 3430 with a FDO® 925 sensor.

For each batch experiment, the sediment-solution suspension was continuously mixed end-over-end on a rotating mixer at 25 revolutions per minute (rpm) for an equilibration time of two days. Depending on the type of experiment, the electrolyte was amended with the stock solutions of As(III) and phosphate (from here on referred to as PO_4) prepared using analytical grade 0.05 M $NaAsO_2$ solution and KH_2PO_4. Light-impermeable brown polypropylene centrifuge tubes were used to prevent photo-catalyzed oxidation of As(III). Experiments were conducted under N_2/H_2 atmosphere in the anaerobic chamber. No attempts were made to suppress microbial activity.

Naturally sorbed concentrations of arsenic and PO_4 on the surface sites of the aquifer sediments were measured as per the sequential extraction scheme (Keon et al., 2001) and the modified Colwell-P method (Rayment & Lyons, 2011), respectively. Naturally sorbed arsenic was extracted by mixing 4.00 g of sediment with 40 mL of 0.5 M NaH_2PO_4 at 25°C for 16 hours. Naturally sorbed PO_4 was extracted from the sediment by mixing 0.40 g of sediment with 0.5 M $NaHCO_3$ at pH 8.5 for 16 hours at 25°C. Samples were centrifuged at 3,500 rpm for 10 min and the supernatants were collected and filtered using a 0.45 μm cellulose acetate membrane filter (Whatman). Supernatants from the PO_4 extractions were treated with 1 M H_2SO_4 and diluted to 50 mL with deionized water for laboratory analysis.

Arsenic sorption experiments were carried out against varying arsenic concentrations, solution pH and PO_4 concentrations. Concentration dependent arsenic adsorption on aquifer sediments, i.e., adsorption isotherms, was determined for 3 batches of 7 samples each (Table 2). The solution pH in each batch was set to 6.10 ± 0.05, 7.51 ± 0.05 and 9.25 ± 0.05; and As(III) concentrations in samples within a batch were varied from 5.00×10^{-7} mol/L to 2.00×10^{-5} mol/L. As(III) adsorbed from the solution was determined from the difference between the initial and the final aqueous concentrations. Arsenic adsorption as a function of pH was measured in 8 samples for an initial As(III) concentration of 2.00×10^{-6} mol/L with solution pH values ranging from 5.70 to 9.85. The pH of each sample was adjusted with ~0.1 and ~1.0 M *HCl* or *NaOH* prior to adding As(III). The influence of PO_4 on arsenic adsorption at pH 9.17 ± 0.10 was determined in 3 batches of 3 samples each. The initial As(III) concentration of each sample in all batches was adjusted to 5.00×10^{-7}, 1.00×10^{-6} and 2.00×10^{-6} mol/L, while the initial PO_4 concentrations of all samples in each batch were adjusted to 1.60×10^{-6}, 3.20×10^{-6} or 6.40×10^{-6} mol/L. The final solution pH after completion of

Table 2
Summary of Laboratory Sorption Experiments

Experiment	Batches	No. of samples per batch	As added (μmol/L)	Solution pH	P as PO_4 added (μmol/L)
Isotherm	#1	7	0, 0.5, 1, 2, 5, 10, 20	9.25 (for all samples)	N/A
	#2	7	0, 0.5, 1, 2, 5, 10, 20	7.51 (for all samples)	N/A
	#3	7	0, 0.5, 1, 2, 5, 10, 20	6.10 (for all samples)	N/A
pH	#1	8	2 (for all samples)	5.70, 6.15, 6.50, 7.00, 7.25, 7.50, 8.50, 9.85	N/A
Competition with P	#1	3	0.5 (for all samples)	9.20 (for all samples)	1.6, 3.2, 6.4
	#2	3	1 (for all samples)	9.20 (for all samples)	1.6, 3.2, 6.4
	#3	3	2 (for all samples)	9.20 (for all samples)	1.6, 3.2, 6.4

sorption experiments was measured using TPS WP-90 with an IJ-44C pH electrode (Ionode). Samples were centrifuged at 4,500 rpm for 10 min and the supernatants were collected and filtered using a 0.45 μm cellulose acetate membrane filter (Whatman) in the dark under anaerobic conditions.

The filtered samples were analyzed for arsenic, iron, aluminum, magnesium, manganese, soluble reactive phosphorus, potassium, silicon and sodium including arsenic speciation for two samples from every experiment at the ChemCentre (Perth, WA). The samples were analyzed using inductively coupled plasma (ICP) – mass spectrometry (MS) and atomic emission spectroscopy (AES); and arsenic speciation was carried out using hydride generation atomic absorption spectroscopy (HGAAS). The soluble reactive phosphorus (P) in the PO_4 extraction samples were measured by the flow injection analysis (method 4500P-G) (American Public Health Association (APHA), 2012). Arsenic speciation measured on selected supernatant samples from each experiment did not detect As(V), thereby confirming that no oxidation of As(III) had occurred during the experiments.

3.2. Observed Geochemical Response

The sediment used in sorption experiments were measured to have naturally sorbed concentrations of 14.24 μmol/kg of arsenic, presumably As(III), and 129 μmol/kg of phosphate, respectively. The adsorption of As(III) onto sediments produced non-linear isotherms under varying pH and As(III) solution concentrations as shown in Figure 2a. Sorption capacity of the sediment was observed to be higher at a pH of 7.51 compared to that at 6.10 and 9.25. This trend was consistent with the results of studies on Fe(III)-oxides (Dixit & Hering, 2003; Pierce & Moore, 1982; Raven et al., 1998), amorphous Al-oxide (Goldberg, 2002), and certain clay minerals (Goldberg, 2002; Manning & Goldberg, 1997a).

Sorption of As(III) onto sediment material over the pH range from 5.70 to 9.85 is shown in Figure 2b. Sorption was observed to increase gradually from pH 5.70 to 7.25, followed by a gradual, then steep decline for pH values above 8.50. As(III) concentration at a solution pH of 9.85 was observed to be higher than the added concentrations suggesting that some of the naturally sorbed As(III) on the sediments was mobilized. The sorption trend observed between a pH of 5.70 and 9.85 was similar to that reported in previous studies conducted with either laboratory synthesized minerals, such as Fe(III)-oxides (Dixit & Hering, 2003; Manning et al., 1998; Pierce & Moore, 1982; Raven et al., 1998; Stachowicz et al., 2006), and amorphous Al-oxide (Goldberg, 2002), or with pure clay minerals (Goldberg, 2002; Manning & Goldberg, 1997a). On the other hand, sorption behavior is known to vary for aquifer sediments sourced from different locations by exhibiting either increasing, decreasing or no effect of increasing solution pH (Manning & Goldberg, 1997b).

Competition for sorption between PO_4 and As(III) at varying solution PO_4 concentrations was not observed (Figure 2c) likely due to the small, yet field-relevant, PO_4 concentrations used in the experiments and an abundance of surface sorption sites on the sediment. Such competition has previously been observed on Fe(III)-oxides (Dixit & Hering, 2003; Jain & Loeppert, 2000; Stachowicz et al., 2008), and on aquifer sediments (Gao et al., 2013; Rathi et al., 2017; Thi Hoa Mai et al., 2014).

3.3. Surface Complexation Model (SCM)

The analytical data obtained from laboratory-based sorption experiments were used to develop a site-specific surface complexation model (SCM) for arsenic. A non-electrostatic generalized composite surface complexation modeling (GC-SCM) (Davis et al., 1998) approach was utilized to account for the inherent

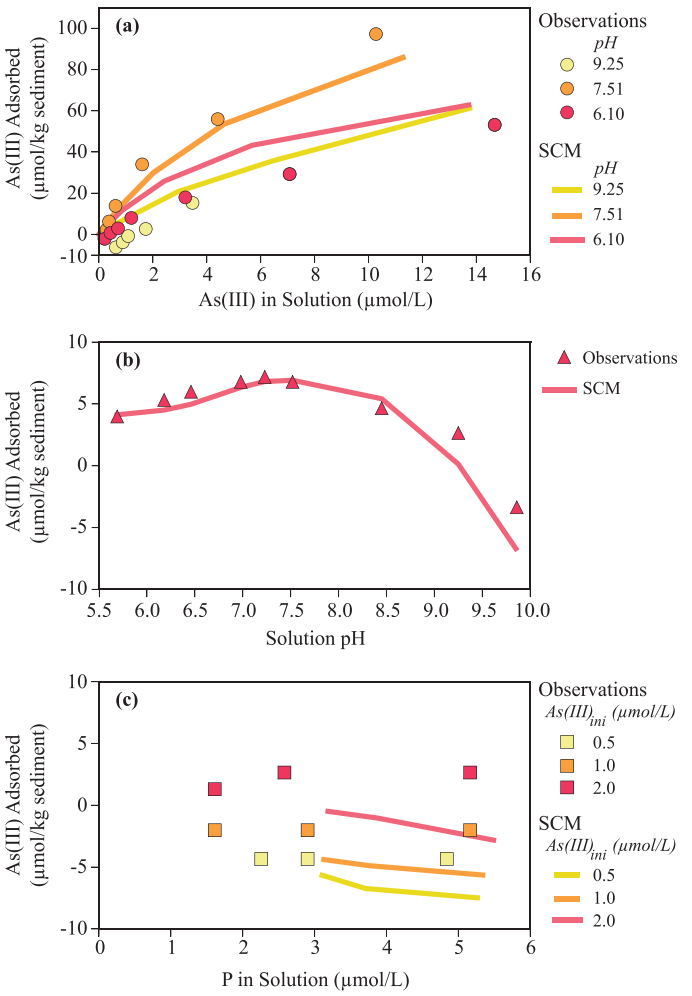

Figure 2. Laboratory As(III) sorption experimental observations and surface complexation model (SCM) simulations. (a) Adsorption of As(III) on aquifer sediment produced non-linear isotherms and demonstrated highest sorption capacity at pH of 7.51. SCM simulations matched the trends for arsenic adsorption with the best model fits observed for data at pH values of 7.51 and 9.25. The simulated output is slightly underestimated at a pH of 7.51, while being overestimated at a pH of 6.10 and 9.25. (b) As(III) sorption with changing solution pH increase gradually from pH 5.70–7.25, followed by a gradual, then steep decline for pH values above 8.50. Some of the naturally sorbed As(III) was mobilized at pH 9.85. SCM captured the effects of solution pH on adsorbed arsenic very accurately. The simulated output demonstrated highest sorption capacity of the sediments around pH 7.50, while no adsorption was observed at pH above 9.50. (c) No competition for sorption between PO_4 and As(III) at varying solution PO_4 concentrations was observed. SCM was able to simulate the lack of competitive effect between arsenic and PO_4 sorption.

physical and chemical heterogeneity of natural sediments without the need for quantification of the surface charge and electric potential of sediment surfaces. The geochemical model PHREEQC v2 (Parkhurst & Appelo, 1999) was used to analyze the data collected from the sorption experiments. A set of surface complexation reactions for arsenic, as As(III), and competing anion PO_4 on a generic surface sorption site, Site_*OH*, were defined in the WATEQ4F database (Ball & Nordstrom, 1991). The GC-SCM parameters included apparent equilibrium constants (log K) and the density of surface sorption sites (m_l) (Table 2). The protonation and dissociation reactions of the surface sorption sites were excluded in the model. All 38 samples from sorption experiments were sequentially simulated in PHREEQC by invoking a batch-type equilibrium reaction step between a given solution composition and the surface, Site_*OH*, at the respective solution pH value. The initial values of the GC-SCM parameters were determined through manual calibration and subsequently, further modified during automated calibration and uncertainty analyses.

4. Field-Scale Reactive Transport Model for Arsenic

At the field-scale, reactive transport of arsenic was simulated to analyze the observations from the injection trial and to predict the long-term behavior of arsenic. In the first step, a non-reactive, conservative version of the model was used to estimate the physical transport processes. Subsequently, reactive transport processes were invoked, while incorporating and upscaling the information gained from the laboratory experiments and associated GC-SCM results.

4.1. Flow, Conservative Solute, and Heat Transport

The numerical flow model was constructed using MODFLOW (Harbaugh, 2005) and subsequent physical transport simulations were performed with PHT3D (Prommer et al., 2003). Measured tracer (*Br*) and conservative species (*Cl*) data were used as the main constraints for calibrating the adjustable physical transport parameters, i.e., the longitudinal (α_L) and transverse (α_T) dispersivities.

As substantial temperature differences occurred between the background groundwater in the Precipice Sandstone (~62°C) and the injected water (~19°C), heat transport was therefore considered (i) as an additional environmental tracer and (ii) to appropriately consider the temperature-dependency of geochemical reactions. In the simulations, temperature was considered as an additional species and heat transport parameters were selected based on the similarities between solute and thermal energy transport, as discussed earlier (Anderson, 2005; Engelhardt et al., 2013; Ma et al., 2012; Seibert et al., 2014). Measured temperature data were used to calibrate the thermal diffusion (D) and thermal distribution (K_d) parameters.

4.1.1. Model Domain and Discretization

The model was set up as a radial-symmetric model under the assumptions that (i) the influence of the background groundwater flow was negligible over the duration of the injection experiment and (ii) that aquifer heterogeneity in lateral direction was not significant. The vertical extent of the model was limited to depths between 1,278 and 1346.5 mBGS, and discretized into 24 layers of varying thickness, porosity and hydraulic conductivity. The vertical discretization was selected to consider the heterogeneity suggested by the wireline logging responses. The Moolayember at depth > 1346.5 m was considered impermeable. Each layer was assumed to be homogenous and continuous in the lateral direction. A log transform was performed to

estimate the hydraulic conductivity of each layer. This was based on a porosity-permeability relationship obtained from a database of publically available petroleum industry data and corrected to match the transmissivity obtained from pumping test analysis of the injection bore (Sreekanth & Moore, 2015). The lateral discretization varied between 1 m, near the injection/extraction well, and 43 m at the column most distant from the well (Figure 3).

Continuously measured injection and extraction rates were discretized into daily steps in the model. The chemical analysis of groundwater samples prior to the start of the injection trial was used to define the background groundwater composition (Table 1), while the regularly measured injectant compositions were used to define the time-varying injectant composition in the model.

4.1.2. Model Parameters

Physical and heat transport parameters were estimated by constraining them with the measured *Br* and *Cl* concentrations as well as measured temperatures. The estimated dispersivity values of α_L =1.29 m and α_T = 0.226 m, and thermal coefficient values of $D = 2.00$ m^2/day and $K_d = 2.00x10^{-4}$ m^3/kg provided a good agreement between simulation results and observations (Figure 4). The good agreement was achieved without invoking a dual-domain approach, which suggests that fracture flow and transport may not occur, or at least not be a dominant feature, within the investigated zone of the Precipice aquifer. A sensitivity analysis also indicated that the resulting parameter estimates were relatively unique and uncorrelated. Therefore, these parameters were assumed to have little impact on the estimation of the parameters controlling geochemical reactions. The estimated dispersivity values were subsequently fixed to their calibrated values for the remainder of this study.

4.2. Reaction Network

The conservative solute transport model was extended to simulate multi-component reactive transport with a primary focus on the processes affecting the fate of arsenic. The most common previously reported mechanisms for arsenic mobilization were (i) the reductive dissolution of Fe(III) (oxy)hydroxides (McArthur et al., 2004; Nickson et al., 2000; Rawson et al., 2017); (ii) co-release of arsenic during the oxidation of Fe-sulfides (Wallis et al., 2010, 2011); and (iii) arsenic desorption from sediment surfaces due to either changing solution pH or competing anions (Smedley & Kinniburgh, 2002). In the present case, reductive dissolution of Fe(III) (oxy)hydroxides was deemed unlikely due to the prevalent reducing conditions (as indicated by the presence of dissolved methane) in the Precipice Sandstone aquifer, which makes it unlikely for a significant fraction of easily-reducible iron minerals to persist. And in case any Fe(III) (oxy)hydroxides still persisted in the highly reducing aquifer, the injectant would have needed to contain a suitable reductant to cause

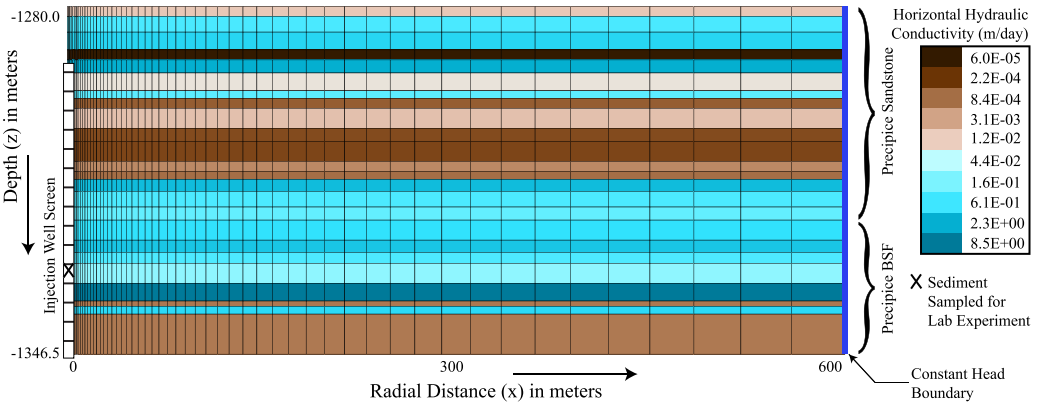

Figure 3. Field-scale groundwater flow model grid. The model was set up as a radial-symmetric model through Precipice sandstone and Precipice BSF layers and model grid was discretized into 24 layers of varying thickness, porosity and hydraulic conductivity. Each layer was assumed to be homogenous and continuous in the lateral direction. Hydraulic conductivity and porosity values of each layer was taken from (Sreekanth & Moore, 2015). The color fill represents the horizontal hydraulic conductivity values along the layers. The lateral discretization varied between 1 m, near the injection/extraction well, and 43 m at the column most distant from the well. Well screen was assigned to the left-most column between depths 1,290 and 1346.5 mBGS. A constant head boundary was assigned to the right-most column. Sediment sample for laboratory sorption experiments was collected at a depth of 1332.53–1333.55 mBGS prior to well construction.

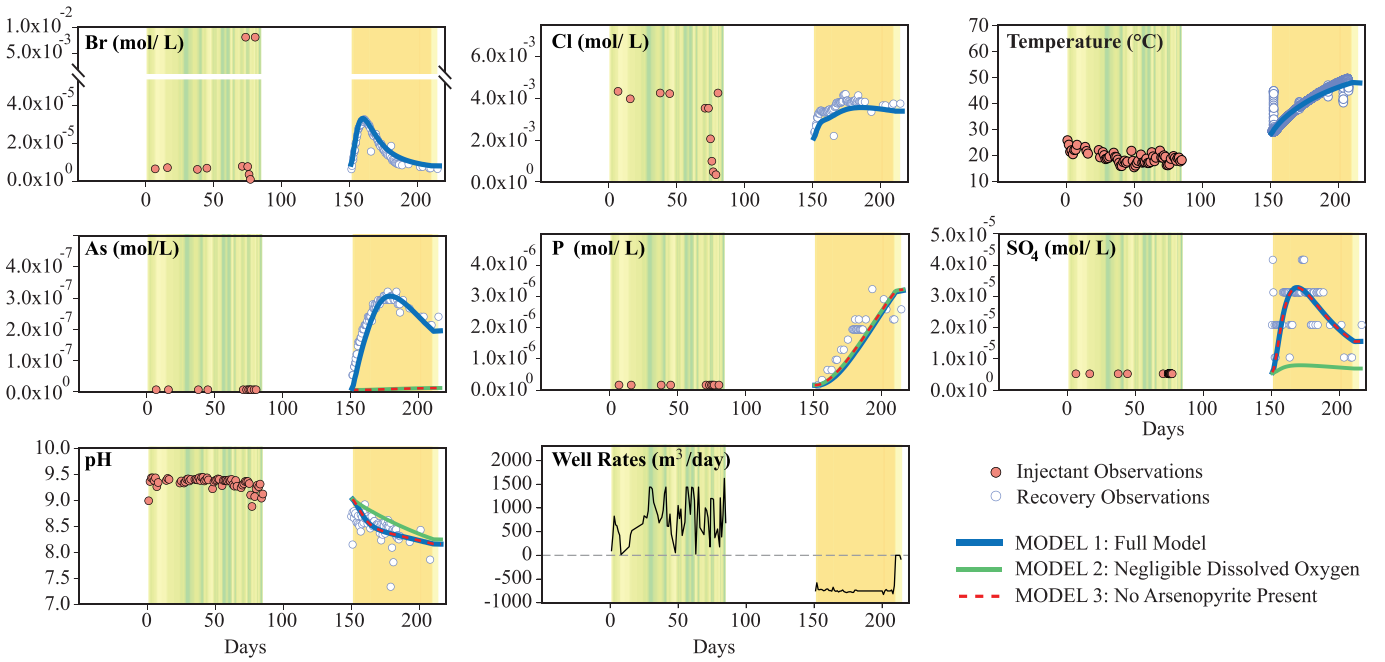

Figure 4. Field injection trial observations and field-scale conservative solute, heat and reactive transport model simulations. CSG co-produced water was injected for 65 days spread over 85 days period, followed by a storage period of 64 days to allow the injected water to react with the native groundwater and the aquifer matrix. Finally, a recovery phase was operated for a total of 309 days. The figure illustrates the injected and the extracted water compositions measured over the injection phase and the first 65 days of the recovery phase, during which most of the injected water was recovered. Continuously measured well injection and extraction rates were discretized into daily steps in the model. The chemical analysis of groundwater samples prior to the start of the injection trial was used to define the background groundwater composition (Table 1), while the regularly measured injectant compositions were used to define the time-varying injectant composition in the model. Calibrated flow model was in good agreement with bromide and chloride concentrations and temperature observations. Physical transport and thermal parameters were fixed to their calibrated values during the reactive transport model (RTM) calibration. In the RTM, arsenic mobilization was modeled using desorption (primary process) and co-release with pyrite oxidation (secondary process). The equilibrium constants in the laboratory-derived SCM were included and kept fixed while an upscaled field surface site density parameter (m_f) was estimated. The pyrite oxidation was simulated using parameter *do* which represented the dissolved oxygen concentrations in the injectant. The arsenopyrite fraction (*aspy*) parameter controlled the co-release of arsenic during pyrite oxidation. The model which included all three parameters (Model 1, blue solid line) produced the best calibration for all the reactive species. Models with either negligible dissolved oxygen in injectant (Model 2, green solid line) or with no arsenopyrite fraction (Model 3, red dashed line) failed to calibrate arsenic observations. Model 2 simulations confirms the occurrence of pyrite oxidation during the injection trial.

further reductive dissolution, which was not the case. Furthermore, co-release of arsenic during the oxidation of Fe-sulfides, e.g., pyrite, was initially considered unlikely since the injectant was deoxygenated and other potential oxidants such as, nitrate or chlorine, were not present. However, sulfate concentrations in the recovered water were observed (4.16×10^{-5} mol/L) in excess of the background value which was at the detection limit of 1.04×10^{-5} mol/L, suggesting that pyrite oxidation may have occurred.

As briefly mentioned above, desorption of arsenic from the sorption sites on sediment surfaces due to the changing solution composition was considered to potentially be the main cause for arsenic mobilization. Arsenic desorption could be caused by either as a result of changes in the solution pH (Dzombak & Morel, 1990), or competing anions, most importantly by PO_4 (Jain & Loeppert, 2000) and HCO_3 (Appelo et al., 2002). The pH in the injectant (avg. 9.30) was significantly above the pH in the background water (avg. 7.86). On the other hand, concentrations of PO_4 in the injectant water were below detection limit (3.23×10^{-7} mol/L) and HCO_3 concentrations in the injectant were below those in the background water. Moreover, the laboratory-based measurement of sediment arsenic sorption characteristics suggest that the change in solution pH could be the primary cause of arsenic mobilization. In the field-scale RTM, arsenic desorption was considered as the primary mechanism for arsenic mobilization by incorporating the surface complexation reactions of As(III) and PO_4 from the laboratory-derived GC-SCM.

Additionally, due to the observed sulfate concentrations in the extracted water, we also considered the possibility of pyrite oxidation:

$$FeS_2 + 3.75O_2 + 3.5H_2O = Fe(OH)_3 + 2SO_4^{2-} + 4H^+ \quad (7)$$

This reaction could have occurred in case of residual dissolved oxygen being contained in the injectant water. This could plausibly explain the occurrence of up to 4.16×10^{-5} mol/L of sulfate in the recovered water. Kinetically controlled pyrite oxidation was modeled as described earlier in (Wallis et al., 2010, 2011):

$$r_{pyr} = \left[\left(C_{o_2}^{0.5} + f_2 C_{NO_3^-}^{0.5}\right) C_{H^+}^{-0.11} \times \left(10^{-10.19} \times \frac{A_{pyr}}{V}\right)\left(\frac{C}{C_0}\right)_{pyr}^{0.67}\right] \quad (8)$$

where, r_{pyr} is the specific oxidation rate for pyrite, C_{O_2}, $C_{NO_3^-}$ and C_{H^+} are the oxygen, nitrate and proton groundwater concentrations, respectively, $\left(\frac{A_{pyr}}{V}\right)$ is the ratio of mineral surface area to solution volume set to 115 $dm^{-1}mol^{-1}$, and $\left(\frac{C}{C_0}\right)$ is a factor that accounts for changes in A_{pyr} resulting from the progressing reaction. Parameter f_2 is a constant, which was assumed to be unity (Eckert & Appelo, 2002; Prommer & Stuyfzand, 2005). Arsenic is often incorporated into the structure of pyrite and has shown to co-dissolve during pyrite oxidation (Jones & Pichler, 2007). This process was considered in our model and the rate of release (r_{aspy}) of arsenic associated with pyrite (i.e., arsenopyrite) oxidation was considered by scaling r_{pyr} with a proportionality term (*aspy*), which represents the molar ratio of arsenic within pyrite:

$$r_{aspy} = aspy \times r_{pyr} \quad (9)$$

The reported values of *aspy* found in pyrite is known to vary considerably from about 0.013 mol% to as high as 4.06 mol% (Welch et al., 2000). The value of *aspy* was not measured for the sediments used in this study and was therefore considered as an unknown parameter in the field-scale RTM and was estimated during the calibration procedure discussed below.

4.3. Upscaling

Upscaling of the laboratory-derived GC-SCM to the field-scale RTM required consideration of the difference in heterogeneities between the two systems. The term heterogeneity here refers to the differences in the total mass of the sediment involved in the two experimental methods, the differences in the solid-solution ratios, the elapsed experimental times, the spatial extent of the two systems, the complexity arising due to the interplay between chemical and physical processes, and the mixing due to advection (Miller et al., 2010). Miller et al. (2010) found that the upscaling was most successful when non-electrostatic GC-SCMs were employed with the differences in heterogeneity between the laboratory and field scale systems being handled by the scaling of the surface area of the sediments. In the literature this has in several instances been achieved through some form of upscaling approach that links the laboratory and field-relevant surface areas of the sediment. For instance, Curtis et al. (2006) estimated the total surface area of aquifer sediments for their uranium transport model by applying a factor based on the porosity and the percentage of the aquifer sediment represented by their laboratory sample. They, along with Davis et al. (2004) and Stollenwerk (1998), also used the reactive surface area for scaling by including additional types of sorption sites to explicitly consider the chemical heterogeneity of mineral surfaces. However, the presence of poorly crystalline phases and surface coatings on the sediment grains can make it difficult to separate reactive surface area from the total area for both idealized, e.g., lab-synthesized, and natural sediments (Arnold et al., 1998, 2001; Lützenkirchen et al., 2002).

In GC-SCMs developed for laboratory batch experimental data, the employed surface area represents an averaged metal(loid) sorption behavior over both the reactive and nonreactive areas on the sediment surface. Upscaling a GC-SCM from laboratory to field scale by modifying the total surface area assumes that (i) the degree of surface heterogeneity of the experimental sediment material used to formulate the SCM is similar to that found in the field, and that (ii) the water-sediment interactions and reactivity will be similar in field conditions compared to lab conditions (Curtis et al., 2004). Based on these assumptions, we derived the surface sorption site density of aquifer sediments in the field-scale RTM (m_f) by applying a proportionality term, or scaling factor (*scf*), to the laboratory-scale surface sorption site density (m_l) such that,

$$m_f = scf \times m_l \quad (10)$$

The value of *scf* was estimated in the calibration of the field-scale RTM against the data collected from the field injection experiment.

5. Model Calibration and Uncertainty Analysis

5.1. Model Calibration

5.1.1. Laboratory-Derived GC-SCM

The laboratory-scale GC-SCM contained seven independent parameters consisting of six surface complexation equilibrium constants (log K) and one laboratory-scale surface site density (m_l). There were a total of 47 observations consisting of aqueous arsenic and phosphate concentrations. All observations from these arsenic sorption experiments were assigned weights that reflect their magnitudes and measurement noise. The optimal parameter set was determined by minimizing an objective function defined as the sum of squared weighted residuals between the observations and their corresponding model-simulated equivalents.

The laboratory GC-SCM is highly nonlinear with a CPU run-time of ~1 s. Therefore, this model is well suited for derivative-free calibration methods such as Markov-Chain Monte Carlo (MCMC) and heuristic methods. For example, the DREAM software (Vrugt et al., 2009) utilizes a variant of the Metropolis-Hastings MCMC method employing differential evolution as a heuristic procedure to enhance algorithmic performance. Another option, known as the Particle Swarm Optimization (PSO) algorithm, is a heuristic method that has shown promise in efficiently finding globally optimal solutions to highly nonlinear optimization problems (Eberhart & Kennedy, 1995). PSO is employed in this study for calibrating the laboratory-scale GC-SCM. Our PSO algorithm was recently parallelized using the YAMR run manager contained within the PEST++ software suite (Welter et al., 2015) similar to the procedure employed by Rawson et al. (2016) and Rathi et al. (2017).

Overall, the calibrated GC-SCM captures the observed data reasonably accurately over the tested concentration range (Figure 2). In the isotherm experiments, model simulations match the trends for arsenic adsorption with the best model fits observed for data at pH values of 7.51 and 9.25. The simulated output is slightly underestimated at a pH of 7.51, while being overestimated at a pH of 6.10 and 9.25 (Figure 2a). The model simulations also capture the effects of solution pH on adsorbed arsenic very accurately. The model output demonstrates that the highest sorption capacity of the sediments is around a pH of 7.50, while no adsorption was observed at pH values above 9.50 (Figure 2b). The model is able to simulate the lack of competitive effect between arsenic and PO_4 sorption, similar to the experimental data (Figure 2c). However, the model calibration is at its worst for these experiments. The simulated output underestimated sorbed arsenic while overestimating the solution PO_4 concentrations. This poor level of model calibration could not be improved, suggesting that the model-structure may contain errors. Addressing model-structure errors was beyond the scope of this study, as it would require further geochemical characterization of the sediment material in order to include additional processes in the conceptual model. However, since the experimental results showed no competition between arsenic and PO_4, no further analysis was deemed critical for the purpose of utilizing the SCM in the field RTM. A calibrated parameter set for the GC-SCM is listed in Table 3. Further examination of the particle positions upon completion of the PSO calibration process suggested that the optimal parameter set is non-unique with several parameters exhibiting strong correlations and mild insensitivity. This correlation and insensitivity is a source of uncertainty that is addressed quantitatively later in this paper.

5.1.2. Field-Scale RTM

The field-scale RTM contains nine parameters consisting of the six surface complexation equilibrium constants (log K) defined in the GC-SCM, the up-scaled field surface site density parameter (m_f), the stoichiometric ratio $As : FeS_2$ that expresses how much arsenic is structurally incorporated into pyrite (*aspy*), and dissolved oxygen concentration (*do*). The latter parameter (*do*) was included to investigate the origin of the elevated sulfate (SO_4) concentrations that were observed during the recovery phase of the field trial. We speculated that the most plausible cause was (i) that the injection of low levels of oxygen may have occurred accidentally, despite the measured oxygen concentrations being consistently below 1.25×10^{-5} mol/L, or (ii) that some other unidentified process with equivalent consequences (i.e., SO_4 and arsenic release) had occurred. A wide range of other conceptual models (e.g., oxidation events during well construction, gypsum dissolution) were also considered but eventually discarded because they were unable to reproduce observed concentration patterns, and are therefore not discussed here.

A total of 151 observations consisting of aqueous arsenic, PO_4, SO_4 concentrations, and pH were available for field-scale RTM calibration. The scaling factor parameter (*scf*) was estimated during the automated calibration and the corresponding field surface site density parameter (m_f) was calculated using equation (10).

The objective function was defined in the same way as discussed previously. However, due to much longer CPU run-times of >1 hour, gradient-based local-search methods were required for the calibration of the field-scale RTM. Therefore the Gauss-Levenberg-Marquardt algorithm contained in the PEST software suite (Doherty, 2016a, 2016b) was employed for this task.

In order to reduce the computational expense associated with calibrating the field-scale RTM to the reactive constituents, and alleviate some of the effects of correlation and insensitivity, the six surface complexation equilibrium constants estimated for GC-SCM were used in the calibration of the field-scale RTM as fixed constants. This reduces the parameter dimension from nine to three, resulting in a very efficient calibration procedure as well as in significant computational reductions for the subsequent predictive uncertainty quantification. Overall, the calibrated field-scale RTM (Model 1) captures the observed data accurately (Figure 4). The calibrated values for *aspy*, *do*, and m_f are 0.0265 (or 2.65 mol%), 1.753×10^{-4} mol/L and 1.647×10^{-6} mol sites, respectively (Table 3).

Although these results reproduce the observed behavior in the field quite well, it is important to evaluate the necessity for the inclusion of the oxidation processes considered in this study. Therefore, two additional field-scale RTM variants were considered. The first variant (Model 2) assumed that no arsenic was present in mineralized-form within the sediment material, thus leaving sorption as the only process to control the release of arsenic and its attenuation. The second variant (Model 3) assumed that the injectant contained a dissolved oxygen concentration of 1.25×10^{-5} mol/L, which is equivalent to the reporting limit of the membrane filter unit used for deoxygenation during the field injection trial. Arsenic mobilization in both model variants is caused by desorption due to the high injectant pH and the modeled concentrations matched the background aqueous arsenic concentrations in the aquifer (Figure 4). These results clearly illustrate that a much better agreement between simulated and measured data is achieved when arsenic is mobilized through desorption from surface sites and in association with a low oxygen-limited rate of pyrite oxidation. All subsequent analysis of field-scale RTM were conducted using Model 1.

Figure 5 shows contour snapshots of the key species of interest in the aquifer derived from the field-scale RTM for simulation times that correspond to a day during the injection (50 days), just after the start of recovery (151 days) and toward the end of the recovery period (215 days). Time-lapse *Br* profiles show the distribution of conservative solute during the injection trial. Due to the tracer injection toward the end of injection phase, *Br* concentrations remain at background levels on Day 50. *Br* has traveled its maximum distance by Day 151 in the most permeable layers and on Day 215 almost all of *Br* has been recovered. The temperature profiles were more evenly distributed with depth due to attenuation of temperature gradients by heat conduction and due to the early arrival of the transient temperature signal in the highly permeable layers. This behavior was also reported by reported by Seibert et al. (2014). The pH depth profiles clearly show that at some depth coinciding with the most permeable layers the injected water traveled more than 80 m laterally. Arsenic distribution patterns are affected by oxidation of arsenopyrite in the zones where dissolved oxygen is transported to by advection. However, arsenic migration in most parts of the model domain was limited to 40 m, largely due to sorption on sites vacated by phosphate, which was displaced by advective flow and the high pH of the injectant. The aqueous arsenic concentration at the well on day 215 (Figure 5), when flux weighted, matched the observed concentration in the pumping well (Figure 4) which shows that the aquifer approached its original conditions near the end of the recovery phase.

5.2. Parameter Uncertainty

The quantification of predictive uncertainty is essential when using the field RTM to quantify the long-term, large-scale fate of arsenic. Predictive uncertainty can stem from two primary sources, (i) parameter error, and (ii) model-conceptual (or model-structural) error. In this study, we focus on parameter error; however, we recognize that model-structure error, while beyond the scope of this study, may also play a role.

The quantification of parameter uncertainty for nonlinear modeling studies is usually accomplished via Monte Carlo techniques (Keating et al., 2010; Siade et al., 2015; Tonkin & Doherty, 2009; Vrugt et al., 2009). This process can be computationally challenging. The level of computational resources required depends on many factors within three general categories, (i) parameter dimension, (ii) the CPU run-time of a single forward model simulation, and (iii) the degree of nonlinearity exhibited between model parameters and the model-simulated equivalents of observations. These three categories can also compound upon one another; for example, if both the parameter dimension and the CPU run-time are large, the cost of

Table 3
Surface Complexation Reactions of As and P and Calibrated GC-SCM and field-Scale RTM Parameters

Solution species	Description	Parameters	Values	Parameter bounds in calibration Lower	Upper
Laboratory GC-SCM parameters					
As(III)	1. Site_$OH + AsO_3^{3-} + 3H^+ =$ Site_$H_2AsO_3 + H_2O$	$logK_1$	44.84	35	46
	2. Site_$OH + AsO_3^{3-} + 2H^+ =$ Site_$HAsO_3^- + H_2O$	$logK_2$	30.48	20	36
	3. Site_$OH + AsO_3^{3-} + H^+ =$ Site_$AsO_3^{2-} + H_2O$	$logK_3$	16.34	12	26
P	4. Site_$OH + PO_4^{3-} + 3H^+ =$ Site_$H_2PO_4 + H_2O$	$logK_4$	32.44	23	35
	5. Site_$OH + PO_4^{3-} + 2H^+ =$ Site_$HPO_4^- + H_2O$	$logK_5$	14.26	12	27
	6. Site_$OH + PO_4^{3-} + H^+ =$ Site_$PO_4^{2-} + H_2O$	$logK_6$	18.16	10	20
Laboratory surface sites Site_*OH* [moles]		m_l	2.050×10^{-5}	5.00×10^{-6}	1.00×10^{-3}
Naturally sorbed arsenic (mol/kg)			1.424×10^{-5}	-	-
Naturally sorbed phosphate (mol/kg)			1.292×10^{-4}	-	-
Field-scale RTM parameters					
Longitudinal dispersivity (m)		α_L	1.29	-	-
Horizontal transverse dispersivity (m)		α_T	0.226	-	-
Thermal diffusion coefficient (m^2/day)		D	2.0		
Thermal distribution coefficient (m^3/kg)		K_d	2.00×10^{-4}		
Pyrite concentration (mol/kg) (Prommer et al., 2016)		pyr	9.275×10^{-2}	-	-
Field surface sites Site_*OH* [moles]		m_f	1.647×10^{-6}	5.00×10^{-8}	1.00×10^{-4}
Arsenic fraction in pyrite (mol%)		$aspy$	2.65	0.5	5.0
Dissolved oxygen [mol/L]		do	1.753×10^{-4}	1.25×10^{-5}	5.00×10^{-4}

uncertainty quantification is increased dramatically. Based on preliminary model results, it was clear that several parameter combinations exhibited insensitivity and moderate correlations (e.g., *aspy* versus m_f). These observations indicate that, even though the effects of model-structural errors are ignored in this study, the predictive uncertainty associated with the use of the field-scale RTM, due to parameter error, is potentially significant and should be quantified.

In this study, we propose a novel, yet relatively simple methodology to overcome some of the computational issues associated with all three of the aforementioned categories. The proposed approach is driven by the simple fact that the CPU run-time of the laboratory-scale model is on the order of ~1s (over 3,000 times faster than the field RTM). Therefore, we propose to use the laboratory model to quantify as much of the parameter uncertainty as possible for the associated parameters, i.e., the six surface complexation equilibrium constants. This is accomplished relatively quickly, resulting in numerous samples of these parameters that calibrate the laboratory-derived GC-SCM within a specified level, which is defined by the weighted least-squares objective function. Subsequently, we incorporate the results of this uncertainty quantification procedure into the field-scale RTM. Since the uncertainty associated with the surface complexation equilibrium constants is already quantified, the number of parameters, or degree of freedom, considered in the field-scale RTM uncertainty analysis is reduced from nine to three. This reduction in parameter dimension dramatically reduces the computational requirement associated with predictive uncertainty quantification performed with the field-scale RTM. The individual steps of this approach are summarized in in Figure 6.

5.2.1. Laboratory GC-SCM Parameter Uncertainty

As for calibration, the characteristics of the laboratory-derived GC-SCM (i.e., highly nonlinear, but short CPU run-time) suggest that derivative-free global-search Monte Carlo techniques should be employed. With our primary goal of this step being to develop a set of parameter samples, rather than a complete description of the posterior probability distribution of parameters, we chose to implement a fast, simple Monte Carlo variant of the PSO algorithm.

The basic PSO algorithm utilizes the socio-cognitive nature of biological swarms to find the solution to a general optimization problem in which a fitness function is minimized (Eberhart & Kennedy, 1995). For calibration, the fitness function is the weighted least-squares objective function. The particle positions in the swarm are defined as their positions in parameter space; in our study this vector space has a dimension of six. Particles "move" randomly through parameter space according to simple rules composed of a social component (based on the best particle in the swarm, the *g*-best position), a cognitive component (based

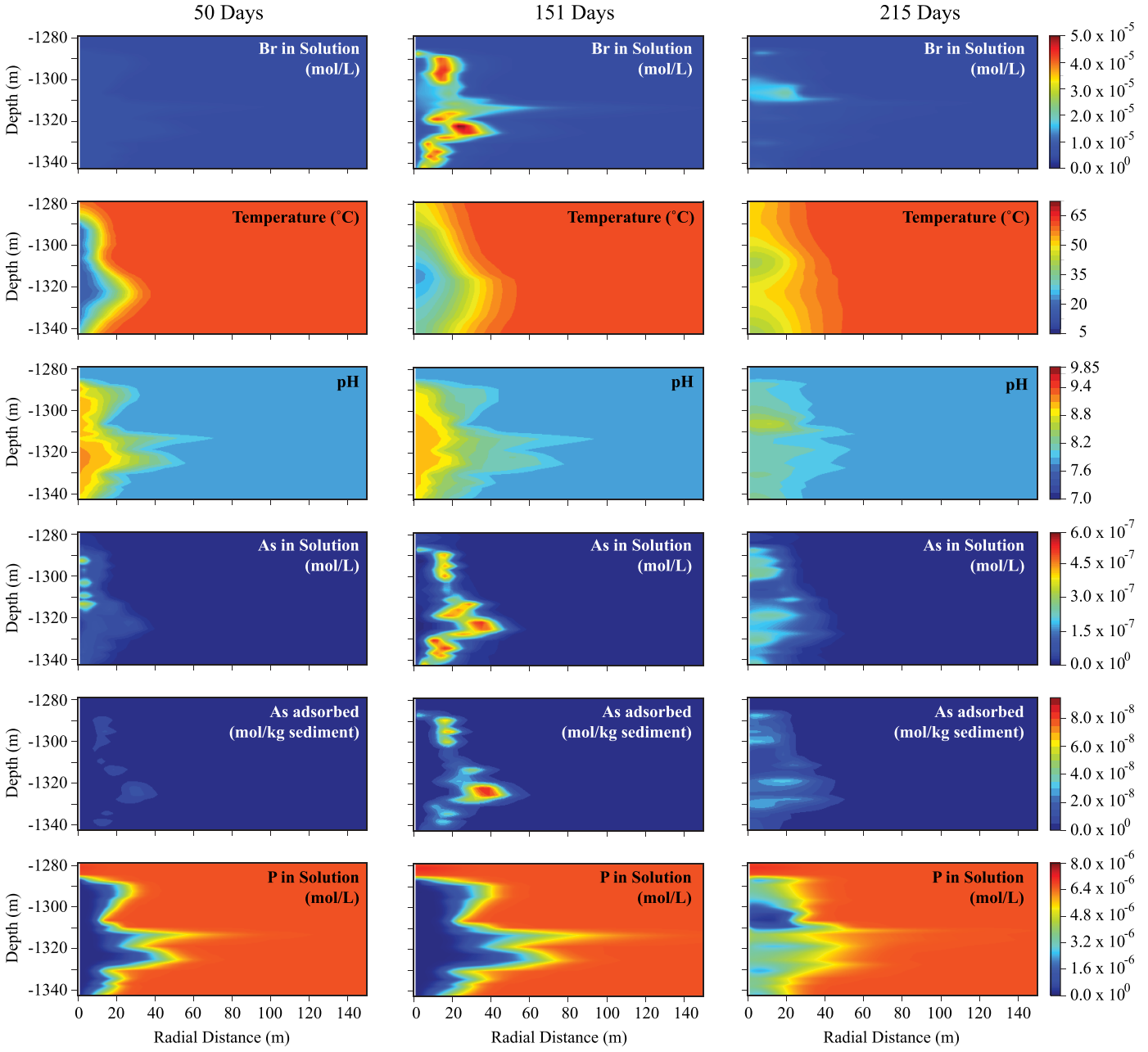

Figure 5. Time-lapse depth profiles in the field-scale RTM. The time-lapse depth profiles of solution bromide, temperature, pH, solution arsenic, adsorbed arsenic, and solution phosphate in the calibrated field-scale RTM at time intervals 50, 151 and 215 days are illustrated here.

on the best performance of the individual particle thus far, the *p*-best position), and the momentum from a previous movement. Convergence is achieved when the particle position with the best fitness function value stops improving.

This PSO algorithm was modified to run in a Monte Carlo mode (Figure 6, Step 1). This is accomplished by simply removing (and saving) particle positions (i.e., parameter values), at a given iteration, that produce a weighted least-squares objective function value below a specified threshold. Once a particle has been removed in this way, a new particle is initialized randomly in its place. The iterative PSO algorithm then proceeds as normal onto the next iteration, where the particles' objective functions are again evaluated, and compared to the specified threshold. This process continues until a desired number of parameter sets have

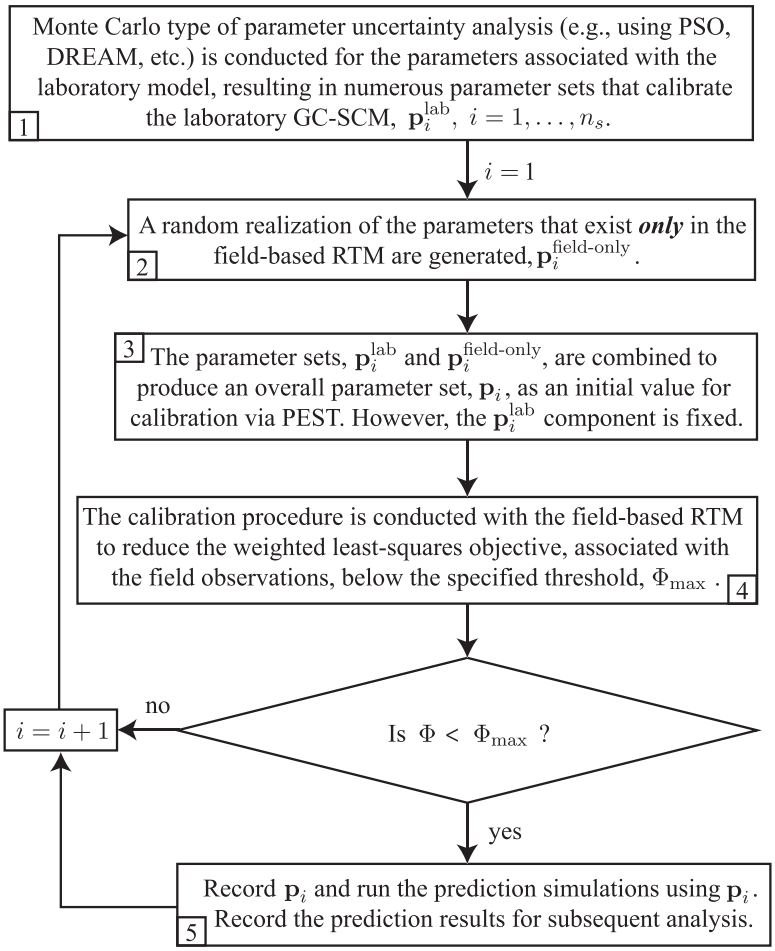

Figure 6. Methodology for model calibration and uncertainty analysis. The parameter set, **p**, consists of all the parameters considered in the field-scale RTM. Some of the parameters in the laboratory-derived GC-SCM will not exist in the parameter set **p**, and vice versa. Therefore, only the parameters from the GC-SCM that also exist in **p** are retained from the parameter uncertainty analysis for the GC-SCM, and comprise the vector $\mathbf{p}^{\text{lab}}$ (i.e., from Step 1). When calibrating the RTM (Steps 3 and 4), the $\mathbf{p}^{\text{lab}}$ component of **p** is fixed since this component already successfully calibrates the GC-SCM and no further calibration is needed. In Step 4, the RTM is calibrated with the scaling factor (*scf*) as a parameter; therefore, the laboratory value for surface site density (m_l) is required from the GC-SCM in order to set the site density for the field model (m_f) during the model calibration process.

been saved. In practice, once the swarm of particles gets "close" to the calibration threshold, this procedure can produce many calibrated parameter samples per iteration. However, it might be biased by the *g*-best particle position if that position remains stagnant for a large number of iterations. This phenomenon is alleviated via two considerations. The momentum (or inertia) of a particle position is reduced if it is close to the threshold; this increases the likelihood that this particle will fall below the threshold quickly. Additionally, neighborhoods are used such that the influence of the *g*-best position on the swarm is reduced, or diffused; this slows the convergence of the algorithm but promotes a more diverse search of the parameter space.

The calibration threshold used for this procedure with the laboratory-derived GC-SCM was set to a value just slightly above the lowest weighted least-squares objective function observed in the calibration (Figure 6, Step 1). The Monte Carlo PSO algorithm was run in parallel across many CPUs using the YAMR run manager in the PEST++ software suite (Welter et al., 2015). The swarm size was set to 100 with a neighborhood size of 10. In just over an hour of execution time on an eight-core desktop computer, 900 parameter sets were obtained, each of which calibrate the laboratory GC-SCM. Basic statistics were also conducted on these parameter results (Table 4). Obtaining a large sample size is important, and considering the computational resources available, 900 parameter sets was deemed sufficient for this study.

Table 4
Basic Sample Statistics for the 900 Realizations of the Monte Carlo Uncertainty Analysis Presented in This Study

Short parameter name	Absolute range		Most likely range		Posterior standard deviation	Posterior relative standard deviation (RSD%)	Correlation coefficients								
	Lower	Upper	Lower	Upper			m_f	*aspy*	*do*	*logK*$_1$	*logK*$_2$	*logK*$_3$	*logK*$_4$	*logK*$_5$	*logK*$_6$
m_f	3.03E-08	5.02E-07	1.25E-07	2.19E-07	7.43E-08	40.39%	1.00								
aspy	1.81E-02	3.74E-02	2.19E-02	2.58E-02	2.61E-03	10.90%	0.73	1.00							
do	1.35E-04	2.16E-04	1.67E-04	1.83E-04	1.17E-05	6.62%	−0.21	−0.76	1.00						
logK$_1$	4.47E+01	4.50E+01	4.47E+01	4.48E+01	5.75E-02	0.13%	−0.23	−0.09	−0.01	1.00					
logK$_2$	2.00E+01	3.39E+01	2.00E+01	2.28E+01	3.58E+00	14.13%	−0.03	0.01	−0.04	0.09	1.00				
logK$_3$	1.20E+01	2.49E+01	1.20E+01	1.46E+01	3.42E+00	19.29%	−0.04	0.00	−0.04	0.29	0.35	1.00			
logK$_4$	3.22E+01	3.27E+01	3.24E+01	3.25E+01	9.69E-02	0.30%	−0.02	−0.04	0.03	0.23	0.12	0.04	1.00		
logK$_5$	1.20E+01	2.42E+01	1.20E+01	1.44E+01	3.12E+00	18.45%	−0.04	−0.01	−0.02	0.15	0.24	0.38	−0.02	1.00	
logK$_6$	1.80E+01	1.83E+01	1.80E+01	1.81E+01	5.31E-02	0.29%	−0.19	−0.10	−0.01	0.85	0.12	0.27	0.31	0.08	1.00

Note. The most likely ranges for the parameters are based on the modal bin ranges of the posterior histogram; each parameter range was divided into 5 bins for this calculation.

The strong correlation observed between GC-SCM parameters $logK_1$ (reaction 1) and $logK_6$ (reaction 6) could be attributed to competition for sorption sites between aqueous species H_3AsO_3 and HPO_4^{2-}, that prevail in the experimental pH range of 7.5 and 9.3. Despite this correlation, these parameters were well constrained by the experimental data and hence their values were very unique (see posterior variance and ranges in Table 4). The parameter values of $logK_3$ (reaction 3) and $logK_5$ (reaction 5) were relatively uncertain most likely due to insensitivity.

5.2.2. Field-Scale RTM Parameter Uncertainty

The results of the parameter uncertainty analysis for the laboratory-derived GC-SCM model were implemented within that for the field-scale RTM using a similar procedure to that used for the calibration; this overall process is also depicted in Figure 6. The procedure begins by selecting a parameter set from the laboratory-based results. This parameter set, which already calibrates the laboratory-derived model, is then implemented in the field-scale RTM as fixed values, with the remaining field-scale RTM parameters assigned random initial values (Steps 2 and 3, Figure 6). The field-scale RTM is then calibrated through a standard PEST operation until the weighted least-squares objective function falls below a specified threshold (Step 4, Figure 6); this threshold is also set just above the best level of calibration achieved (Figures 4). There are only three parameters to estimate, yet this calibration step still requires up to about 30 hrs to complete (in serial). This process is then repeated for the 900 parameter sets obtained in the laboratory-based uncertainty analysis. All 900 of these Monte Carlo realizations were executed in parallel on the CSIRO high-performance cluster, Pearcey. Overall, the process, including queueing, required about one week of computing time to complete, which is a more practical time compared to what would be required to address all nine parameters using the field-scale RTM.

Basic statistics were conducted on the results of this analysis and presented in Table 4. The field-scale RTM parameters *do* and *aspy* were moderately negatively correlated (correlation coefficient = −0.76); however, simulated sulfate concentrations were only controlled by the value of *do*, which despite this correlation, results in a relatively unique estimate for this parameter (Table 4). The parameters m_f and *aspy* were also moderately positively correlated (correlation coefficient = 0.73); however, in contrast to *do*, this correlation has caused these parameters to be relatively uncertain (Table 4). All surface complexation equilibrium constants are relatively uncorrelated with the three field-scale parameters. This, combined with the fact that all of the surface complexation equilibrium constants obtained from the laboratory-based uncertainty analysis were able to produce an acceptable level of calibration for the field-scale RTM, confirms that these parameters are relatively insensitive to the field-scale RTM model outputs. This further emphasizes the importance of conducting site-specific laboratory experiments followed by the development and analysis of their corresponding GC-SCM.

5.3. Predictive Uncertainty–Long-Term Fate of Arsenic

The results of the parameter uncertainty analysis were used to quantify the predictive uncertainty associated with the long-term fate of arsenic, i.e., over several years of reinjection. In practice there are numerous

Table 5
Injectant Compositions for Predictive Model

Analyte	Background	Injectant 1	Injectant 2
Na (mol/L)	7.74×10^{-3}	4.05×10^{-3}	4.05×10^{-3}
Cl (mol/L)	2.80×10^{-3}	2.06×10^{-3}	2.06×10^{-3}
HCO_3 (mol/L)	2.59×10^{-3}	9.70×10^{-4}	9.70×10^{-4}
pH	7.80	9.34	9.34
Temperature (°C)	62	18	18
Si (mol/L)	5.44×10^{-4}	2.55×10^{-5}	2.55×10^{-5}
SO_4 (mol/L)	5.21×10^{-6}	5.21×10^{-6}	5.21×10^{-6}
Reactive P (mol/L)	6.60×10^{-6}	1.61×10^{-7}	1.61×10^{-7}
As (mol/L)	1.60×10^{-8}	6.67×10^{-9}	6.67×10^{-9}
Dissolved Oxygen (mol/L)	Not measured	1.328×10^{-4}	1.25×10^{-5}

predictions that could be of interest; for example, (i) the maximum (peak) concentration observed at a particular location, (ii) the arsenic behavior under varying, controllable geochemical conditions, (iii) the radius of influence associated with arsenic concentrations that are above specific guidelines, etc.

In this study, we constructed a predictive model for the study site by modifying the model domain that was used for simulating the injection trial. While the overall lateral and vertical extents and the vertical discretization of the model remained unchanged, the discretization in lateral direction was coarsened near the injection well to reduce computational costs. For simplicity a constant injection rate was assigned to simulate the impacts of a long-term injection. The background groundwater composition remained unchanged from the injection trial simulations. Model simulations were derived for all 900 parameter sets produced in the previously discussed Monte Carlo realizations. Simulation results are illustrated by vertically integrating the simulated values over the model domain at each location using transmissivity-weighted averaging.

Two different injectant compositions were employed to examine the fate and transport of arsenic (Table 5). The first injectant composition was similar to that used in the injection trial except that the dissolved oxygen concentration was allowed to change as per the value of parameter *do* obtained during Monte Carlo simulations. For the second tested injectant water composition it was assumed that the dissolved oxygen levels will consistently remain at 1.25×10^{-5} mol/L, corresponding to the specified maximum residual oxygen concentration after de-oxygenation via membrane filters.

5.3.1. Implications for Long-Term Arsenic Behavior: Temporal and Spatial Changes

The results of the predictive model simulations are presented for the simulation completed at the end of 10 years as an example. The results of all 900 predictive model simulations are illustrated in Figure 7, showing the distribution of arsenic moving through the aquifer at this time. There is considerable variability for all 900 simulations; however, these simulations show that the magnitude of arsenic concentrations may exceed the Australian drinking water guideline (1.33×10^{-7} mol/L) at some locations within the aquifer while remaining below the ANZECC (2000) water quality guideline for livestock (6.67×10^{-6} mol/L). Figure 7 also illustrates some aspects of the probability distribution of arsenic at a given distance from the injection well. The mean arsenic concentration, and it's associated +/- one standard deviation, appear closer to the minimum values for the first 350m of the profile and then beyond this point, they appear midway between the lowest and the highest values. The other constituents also show that most of the Monte Carlo simulations reside near the minimum simulated values except for pH which resides more symmetrically between the minimum and maximum simulated values. The variability seen in the groundwater pH and sorbed concentrations of arsenic and PO_4 is overall relatively high by comparison. The increased uncertainty in groundwater pH over the long-term injection was mostly a result of parametric uncertainty in the parameter *do* which controls pyrite oxidation in the model and thus affects solution pH (equation (7)).

Additionally, simulation results are also depicted in Figure 7 that illustrate the effects of the correlation between m_f and *aspy* on predictive uncertainty. The latter parameter controls the amount of arsenic release due to oxidation while the former is responsible for retardation through sorption. The model simulation for higher values of both parameters corresponds to increased arsenic mobilization near the well, which dissipates sharply beyond 350 m due to increased sorption. Intuitively, smaller values of these parameters results in lesser mobilization of arsenic near the well, however, decreased sorption also results in lower

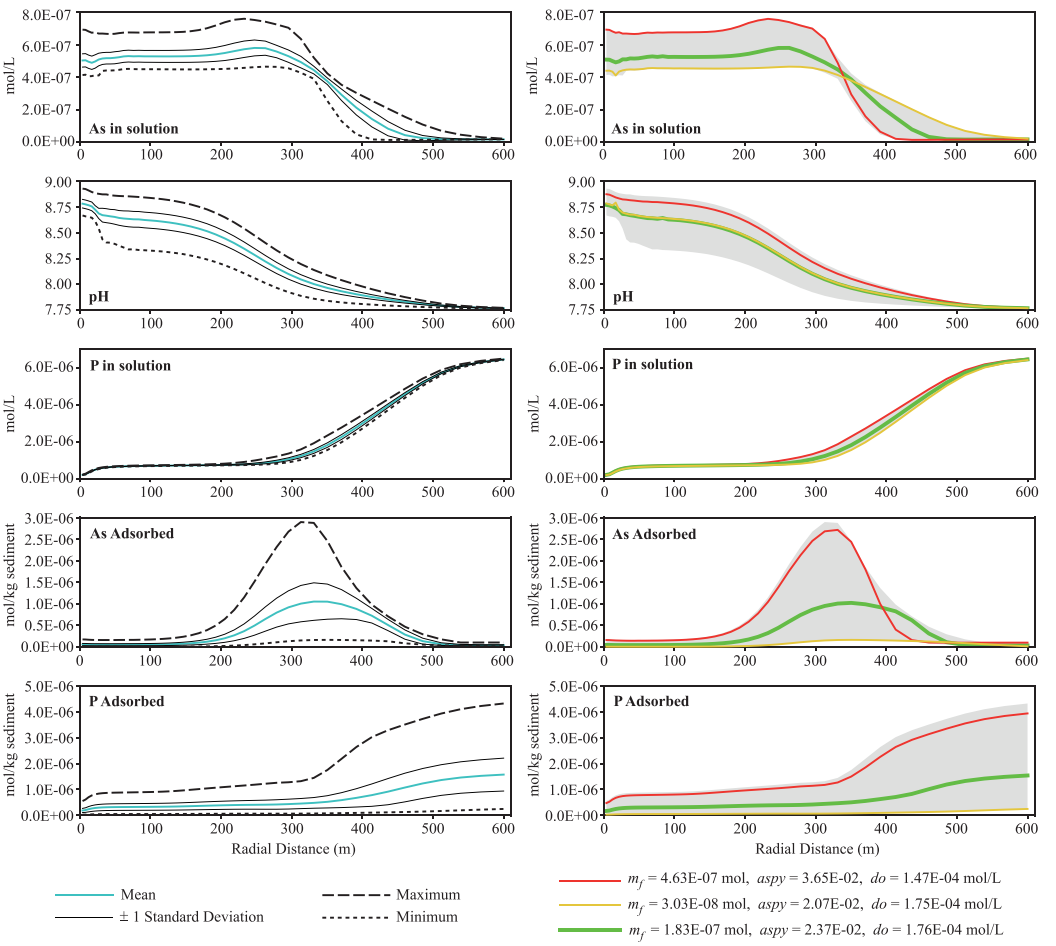

Figure 7. Predictive uncertainty for aquifer injection at the end of 10 years––Part 1. The results of 900 predictive model simulations were produced using injectant composition similar to that used in the injection trial with increased dissolved oxygen concentration of 1.753×10^{-4} mol/L (derived from the calibrated field-scale RTM). The plots on the left illustrate some aspects of the probability distribution of different species at a given distance from the injection well. All 900 simulations are illustrated by the grey shaded area in the plots on the right. Three simulations were selected to demonstrate the effects of correlation between field-scale RTM parameters. The simulation plotted as red line controls arsenic mobility through sorption while the simulation in yellow was dominated by dissolved oxygen parameter (*do*). The simulation in green has similar *do* value as in the yellow simulation and thus clearly shows correlation between field surface site density (m_f) and arsenopyrite fraction (*aspy*) parameters.

retardation over the length of model domain. The simulation results produced by one of the modal parameter sets, i.e., a parameter set with high likelihood based on the posterior histogram (Table 4), represent a highly likely prediction of the model. As shown in Figure 7, this result suggests relatively low arsenic mobilization and stronger retardation.

5.3.2. Implications for Long-Term Arsenic Behavior: Effects of De-Oxygenation

The simulation results of the predictive model discussed above were also produced to test for the effects of a nearly complete de-oxygenation of the injectant on the fate and transport of arsenic (Figure 8). The mean concentrations and the associated +/− one standard deviation of all constituents appear closer to the minimum values. These results also indicate that the magnitude of arsenic mobilized will be reduced dramatically if the dissolved oxygen concentrations in the injectant remain limited throughout the operation of the injection scheme and will remain below the ANZECC (2000) water quality guideline for livestock (6.67×10^{-6} mol/L). Although the overall uncertainty of the model simulations remains similar, the shape of dissolved arsenic migration profile is narrower with smaller peaks. This shape is controlled mainly by sorption processes, and any arsenic mobilization due to oxidation is limited due to the lack of dissolved oxygen in

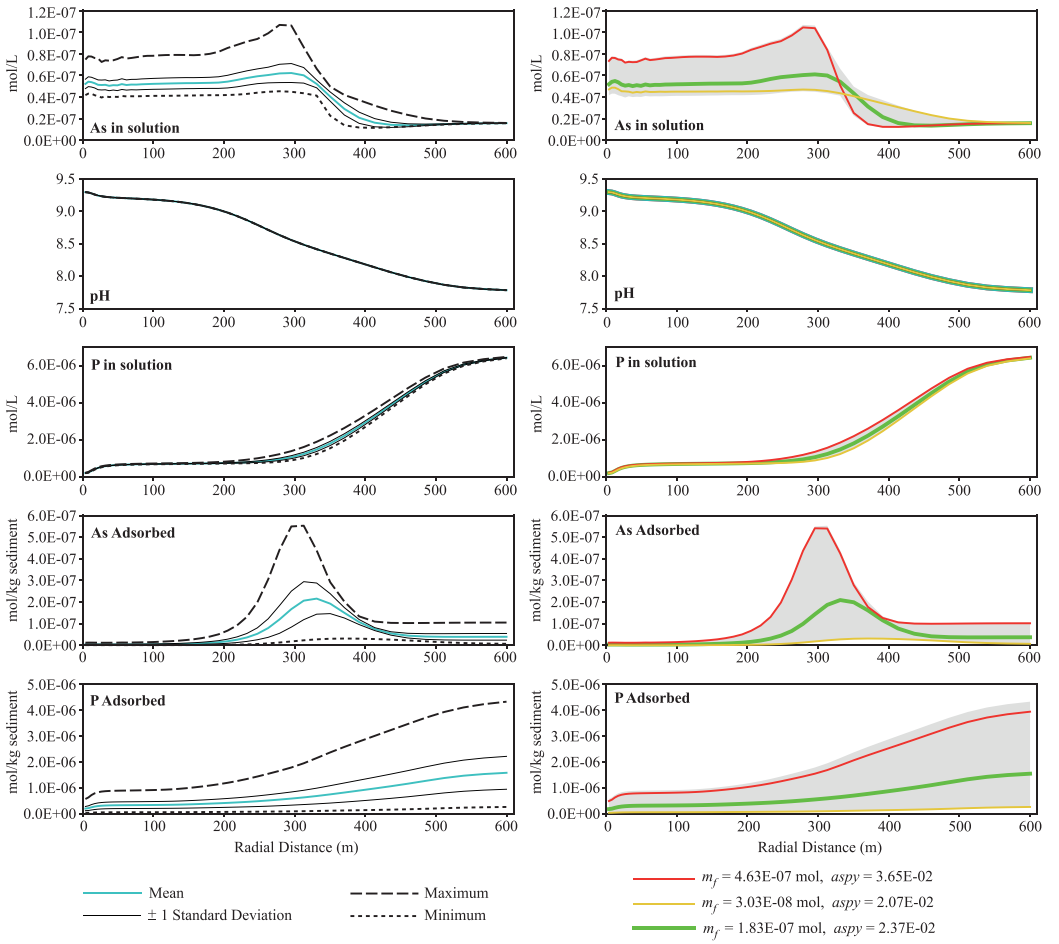

Figure 8. Predictive uncertainty for aquifer injection at the end of 10 years––Part 2. The results of 900 predictive model simulations were produced using injectant composition similar to that used in the injection trial but with nearly complete de-oxygenation of the injectant. The overall results were similar to that illustrated in Figure 7 except that the magnitude of arsenic mobilized was reduced dramatically emphasizing the need for maintaining low levels of dissolved oxygen in the injectant. Note that the results are plotted at different scales to that in Figure 7 to clearly demonstrate the predictive uncertainty where required.

the injectant. These results emphasize the need for maintaining low levels of dissolved oxygen in the injectant.

The predictive analyses discussed above are based only on the key geochemical processes identified in the calibration procedure. It is important to note that the slow geochemical processes not included in the calibration could become increasingly important over the timescale considered in predictive scenarios and these must be understood before carrying out a broader scale predictive analysis for the impact of a larger scale injection scheme.

6. Conclusions

CSG production in coming decades will likely involve the management of large amounts of co-produced water through disposal into deep aquifers after off-site treatment. Prior to the implementation of long-term injection schemes it is important to perform field injection trials that generate sufficiently meaningful data sets to allow for the assessment of both the hydrological and geochemical impacts. The substantial depth of some of the aquifers targeted for reinjection schemes limits the opportunities for an extensive monitoring network and often a push-pull test, as discussed in this study, is the only feasible option to acquire such data sets. The present work illustrates how reactive transport models (RTM) can be used to maximize the

value of the acquired injection trial data in conjunction with multiscale data from supporting laboratory experiments and the pre-trial hydrogeological and geochemical investigations.

During the injection trial analyzed in this study, excess arsenic concentrations (up to 3.20×10^{-7} mol/L) were observed in the recovery phase, suggesting that arsenic was mobilized by the injectant water. The data set collected during this trial allowed for a detailed analysis of the coupled transport and reaction processes. Complementing the data collected in the field, a series of experiments was performed in the laboratory with sediments from the study site to better understand and quantify arsenic sorption behavior. The laboratory data were described by a generalized composite surface complexation model (GC-SCM), which was subsequently incorporated into the field-scale simulations of the injection trial. Upscaling of the GC-SCM from the laboratory to the field scale was achieved by adjusting the surface site density term through a scaling factor. Initially, it was assumed that the mobilization of arsenic was caused primarily by desorption from high injectant pH (9.30). However, due to the observed increase of sulfate concentrations during recovery, it was speculated that pyrite oxidation may have occurred, resulting in the co-release of arsenic incorporated into the pyrite structure. Based on the insights gained from the model calibration we conclude that both desorption and pyrite oxidation may have contributed to arsenic mobilization during the injection trial.

Although it was considered likely that both processes played a role, the magnitude of each process's contribution was highly uncertain due to the high degree of correlation between their respective governing parameters. To account for this uncertainty in the predictions of the long-term arsenic behavior a novel yet simple methodology was developed and presented. The proposed methodology integrates information from both the laboratory GC-SCM and the field-scale RTM into the model predictions. The computational requirements to quantify predictive uncertainty are reduced by exploiting the extremely fast model execution times associated with the GC-SCM. The results indicate that there is a significant uncertainty associated with the long-term fate of arsenic at the study site. However, the results also clearly illustrate that arsenic levels will remain below the Australian drinking water guideline (1.33×10^{-7} mol/L) if the potential for pyrite oxidation is minimized through complete deoxygenation of the injectant. The proposed efficient modeling and predictive uncertainty quantification method can be easily implemented for a wide range of other groundwater studies that investigate the risks of metal(loid) or radionuclide contamination, and can be easily extended to incorporate additional expert knowledge such as, expected trends in parameters, expected ratios amongst parameters, etc.

Acknowledgments
The authors thank Origin Energy as upstream operator of Australia Pacific LNG for the use of their extensive field data set. H.P. and M.D. thank the Gas Industry Social & Environment Research Alliance (GISERA) of Australia for the support of this study. Financial support for B.R. was provided through a University of Western Australia postgraduate research scholarship. The laboratory and computational resources were provided by CSIRO Land and Water, which is gratefully acknowledged. The authors declare no real or perceived financial conflicts of interests in the study. All the data presented in this study is available to download from CSIRO Data Access Portal (DOI: http://doi.org/10.4225/08/59e079f75f7c2) and any additional information can be obtained by contacting the corresponding author.

References

Anderson, M. P. (2005). Heat as a ground water tracer. *Ground Water*, *43*(6), 951–968. https://doi.org/10.1111/j.1745-6584.2005.00052.x

ANZECC (2000). *Australia and New Zealand guidelines for fresh and marine water quality*. Australian and New Zealand Environment and Conservation Council, Agriculture and Resource Management Council of Australia and New Zealand.

American Public Health Association (APHA). (2012). *Standard methods for the examination of water and wastewater* (22nd ed.). Washington, DC: American Public Health Association. Retrieved from http://www.standardmethods.org/

Appelo, C. A. J., Van Der Weiden, M. J. J., Tournassat, C., & Charlet, L. (2002). Surface complexation of ferrous iron and carbonate on ferrihydrite and the mobilization of arsenic. *Environmental Science and Technology*, *36*(14), 3096–3103.

Appelo, C. A. J., & Vet, W. W. J. M. (2003). Modeling in situ iron removal from groundwater with trace elements such as As. In A. H. Welch & K. G. Stollenwerk (Eds.), *Arsenic in ground water: Geochemistry and occurrence* (pp. 381–401). Boston, MA: Springer US. https://doi.org/10.1007/0-306-47956-7_14

Arnold, T., Zorn, T., Bernhard, G., & Nitsche, H. (1998). Sorption of uranium(VI) onto phyllite. *Chemical Geology*, *151*(1–4), 129–141. https://doi.org/10.1016/S0009-2541(98)00075-8

Arnold, T., Zorn, T., Zänker, H., Bernhard, G., & Nitsche, H. (2001). Sorption behavior of U(VI) on phyllite: Experiments and modeling. *Journal of Contaminant Hydrology*, *47*(2–4), 219–231. https://doi.org/10.1016/S0169-7722(00)00151-0

Ball, J. W., & Nordstrom, D. K. (1991). *User's manual for WATEQ4F, with revised thermodynamic data base and text cases for calculating speciation of major, trace, and redox elements in natural waters* (Version 2.). *Open-File Report*. Retrieved from http://pubs.er.usgs.gov/publication/ofr91183

Clarkson, C. R., & Bustin, M. (2011). Coalbed methane: Current field-based evaluation methods. *SPE Reservoir Evaluation and Engineering*, *14*(1), 60–75. https://doi.org/10.2118/131791-PA

Curtis, G. P., Davis, J. A., & Naftz, D. L. (2006). Simulation of reactive transport of uranium(VI) in groundwater with variable chemical conditions. *Water Resources Research*, *42*, W04404. https://doi.org/10.1029/2005WR003979

Curtis, G. P., Fox, P., Kohler, M., & Davis, J. A. (2004). Comparison of in situ uranium KD values with a laboratory determined surface complexation model. *Applied Geochemistry*, *19*(10), 1643–1653. https://doi.org/10.1016/j.apgeochem.2004.03.004

Davis, J. A., Coston, J. A., Kent, D. B., & Fuller, C. C. (1998). Application of the surface complexation concept to complex mineral assemblages. *Environmental Science & Technology*, *32*(19), 2820–2828. https://doi.org/10.1021/es980312q

Davis, J. A., Meece, D. E., Kohler, M., & Curtis, G. P. (2004). Approaches to surface complexation modeling of uranium(VI) adsorption on aquifer sediments. *Geochimica Et Cosmochimica Acta*, *68*(18), 3621–3641. https://doi.org/10.1016/j.gca.2004.03.003

Dixit, S., & Hering, J. G. (2003). Comparison of arsenic (V) and arsenic (III) sorption onto iron oxide minerals: Implications for arsenic mobility. *Environmental Science & Technology*, *37*(18), 4182. https://doi.org/10.1021/es030309t

DNRM (2016). *Underground water impact report for the Surat cumulative management area*. Brisbane, QLD: Department of Natural Resources and Mines, Government of Queensland.

Doherty, J. E. (2016a). *Model-independent parameter estimation user manual Part I: PEST. SENSAN and global optimisers*. Brisbane, QLD: Watermark Numerical Computing.

Doherty, J. E. (2016b). *Model-independent parameter estimation user manual Part II: PEST utility support software*. Brisbane, QLD: Watermark Numerical Computing.

Dzombak, D. A., & Morel, F. M. M. (1990). *Surface complexation modeling-hydrous ferric oxide*. John Wiley.

Eberhart, R., & Kennedy, J. (1995). A new optimizer using particle swarm theory. In *Proceedings of the sixth international symposium on micro machine and human science, 1995, MHS '95* (pp. 39–43). https://doi.org/10.1109/MHS.1995.494215

Eckert, P., & Appelo, C. A. J. (2002). Hydrogeochemical modeling of enhanced benzene, toluene, ethylbenzene, xylene (BTEX) remediation with nitrate. *Water Resources Research*, *38*(8), 1130. https://doi.org/10.1029/2001WR000692

Engelhardt, I., Prommer, H., Moore, C., Schulz, M., Schüth, C., & Ternes, T. A. (2013). Suitability of temperature, hydraulic heads, and acesulfame to quantify wastewater-related fluxes in the hyporheic and riparian zone. *Water Resources Research*, *49*, 426–440. https://doi.org/10.1029/2012WR012604

Exon, N. F. (1976). Geology of the Surat Basin in Queensland. In *Geology and geophysics* (Bulletin 166). Canberra: Australian Government Publishing Service.

Gao, X., Su, C., Wang, Y., & Hu, Q. (2013). Mobility of arsenic in aquifer sediments at Datong Basin, northern China: Effect of bicarbonate and phosphate. *Journal of Geochemical Exploration*, *135*, 93–103. https://doi.org/10.1016/j.gexplo.2012.09.001

Goldberg, S. (2002). Competitive adsorption of arsenate and arsenite on oxides and clay minerals. *Soil Science Society of America Journal*, *66*(2), 413–421. Retrieved from http://search.proquest.com/docview/216061813?accountid=26957

Green, P. M., Carmichael, D. C., Brain, T. J., Murray, C. G., McKellar, J. L., Beeston, J. W., & Gray, A. R. G. (1997). *The Surat and Bowen Basins*. In P. M. Green (Ed.), *South-east Queensland in Queensland Minerals and Energy Review Series* (Vol. 1). Queensland Geological Survey.

Hamawand, I., Yusaf, T., & Hamawand, S. G. (2013). Coal seam gas and associated water: A review paper. *Renewable and Sustainable Energy Reviews*, *22*, 550–560. https://doi.org/10.1016/j.rser.2013.02.030

Harbaugh, A. W. (2005). MODFLOW-2005: The U.S. Geological Survey modular ground-water model - the ground-water flow process. In *Book 6: Modeling techniques, section A. Ground-water*. Retrieved from http://purl.access.gpo.gov/GPO/LPS96824

Jain, A., & Loeppert, R. H. (2000). Effect of Competing Anions on the Adsorption of Arsenate and Arsenite by Ferrihydrite. *Journal of Environmental Quality*, *29*(5), 1422–1430. https://doi.org/10.2134/jeq2000.00472425002900050008x

Jones, G. W., & Pichler, T. (2007). Relationship between pyrite stability and arsenic mobility during aquifer storage and recovery in southwest central Florida. *Environmental Science & Technology*, *41*(3), 723–730. https://doi.org/10.1021/es061901w

Keating, E. H., Doherty, J., Vrugt, J. A., & Kang, Q. (2010). Optimization and uncertainty assessment of strongly nonlinear groundwater models with high parameter dimensionality. *Water Resources Research*, *46*, W10517. https://doi.org/10.1029/2009WR008584

Kent, D. B., Abrams, R. H., Davis, J. A., Coston, J. A., & LeBlanc, D. R. (2000). Modeling the influence of variable pH on the transport of zinc in a contaminated aquifer using semiempirical surface complexation models. *Water Resources Research*, *36*(12), 3411–3425. https://doi.org/10.1029/2000WR900244

Keon, N. E., Swartz, C. H., Brabander, D. J., Harvey, C., & Hemond, H. F. (2001). Validation of an arsenic sequential extraction method for evaluating mobility in sediments. *Environmental Science & Technology*, *35*(13), 2778–2784. https://doi.org/10.1021/es001511o

Lützenkirchen, J., Boily, J.-F., Lövgren, L., & Sjöberg, S. (2002). Limitations of the potentiometric titration technique in determining the proton active site density of goethite surfaces. *Geochimica et Cosmochimica Acta*, *66*(19), 3389–3396. https://doi.org/10.1016/S0016-7037(02)00948-1

Ma, R., Zheng, C., Liu, C., Greskowiak, J., Prommer, H., & Zachara, J. M. (2014). Assessment of controlling processes for field-scale uranium reactive transport under highly transient flow conditions. *Water Resources Research*, *50*, 1006–1024. https://doi.org/10.1002/2013WR013835

Ma, R., Zheng, C., Zachara, J. M., & Tonkin, M. (2012). Utility of bromide and heat tracers for aquifer characterization affected by highly transient flow conditions. *Water Resources Research*, *48*, W08523. https://doi.org/10.1029/2011WR011281

Manning, B. A., Fendorf, S. E., & Goldberg, S. (1998). Surface structures and stability of Arsenic(III) on Goethite: Spectroscopic evidence for inner-sphere complexes. *Environmental Science & Technology*, *32*(16), 2383–2388. https://doi.org/10.1021/es9802201

Manning, B. A., & Goldberg, S. (1997a). Adsorption and stability of Arsenic(III) at the clay mineral−water interface. *Environmental Science & Technology*, *31*(7), 2005–2011.

Manning, B. A., & Goldberg, S. (1997b). Arsenic(III) and arsenic(V) adsorption on three California soils. *Soil Science*, *162*(12), 886–895. Retrieved from http://journals.lww.com/soilsci/Fulltext/1997/12000/ARSENIC_III__AND_ARSENIC_V__ADSORPTION_ON_THREE.4.aspx

McArthur, J. M., Banerjee, D. M., Hudson, E. K. A., Mishra, R., Purohit, R., Ravenscroft, P., . . . Chadha, D. K. (2004). Natural organic matter in sedimentary basins and its relation to arsenic in anoxic ground water: The example of West Bengal and its worldwide implications. *Applied Geochemistry*, *19*(8), 1255–1293. https://doi.org/10.1016/S0883-2927(04)00054-X|10.1016/j.apgeochem.2004.02.001

McNab, W. W., Jr., Singleton, M. J., Moran, J. E., & Esser, B. K. (2009). Ion exchange and trace element surface complexation reactions associated with applied recharge of low-TDS water in the San Joaquin Valley, California. *Applied Geochemistry*, *24*(1), 129–137. https://doi.org/10.1016/j.apgeochem.2008.11.009

Miller, A. W., Rodriguez, D. R., & Honeyman, B. D. (2010). Upscaling sorption/desorption processes in reactive transport models to describe metal/radionuclide transport: A critical review. *Environmental Science & Technology*, *44*(21), 7996–8007. https://doi.org/10.1021/es101822v

Neil, C. W., Yang, Y. J., & Jun, Y.-S. (2012). Arsenic mobilization and attenuation by mineral-water interactions: Implications for managed aquifer recharge. *Journal of Environmental Monitoring*, *14*(7), 1772–1788. https://doi.org/10.1039/C2EM30323J

Nickson, R. T., McArthur, J. M., Ravenscroft, P., Burgess, W. G., & Ahmed, K. M. (2000). Mechanism of arsenic release to groundwater, Bangladesh and West Bengal. *Applied Geochemistry*, *15*(4), 403–413. https://doi.org/10.1016/S0883-2927(99)00086-4

Parkhurst, D. L., & Appelo, C. A. J. (1999). *User's guide to PHREEQC (version 2) a computer program for speciation, batch-reaction, one-dimensional transport, and inverse geochemical calculations* (Vol. xiv). U.S. Geological Survey, Earth Science Information Center; Open-File Reports Section distributor.

Pierce, M. L., & Moore, C. B. (1982). Adsorption of arsenite and arsenate on amorphous iron hydroxide. *Water Research*, *16*(7), 1247–1253. https://doi.org/10.1016/0043-1354(82)90143-9

Prommer, H., Barry, D. A., & Zheng, C. (2003). MODFLOW/MT3DMS-based reactive multicomponent transport modeling. *Ground Water*, *41*(2), 247–257. https://doi.org/10.1111/j.1745-6584.2003.tb02588.x

Prommer, H., Rathi, B., Donn, M., Siade, A., Wendling, L., Martens, E., & Patterson, B. (2016). *Geochemical response to reinjection*. Retrieved from https://gisera.csiro.au/wp-content/uploads/2017/01/GISERA_Project_1_Geochemical_Response_Final_201610.pdf

Prommer, H., & Stuyfzand, P. J. (2005). Identification of temperature-dependent water quality changes during a deep well injection experiment in a pyritic aquifer. *Environmental Science & Technology*, *39*(7), 2200–2209. https://doi.org/10.1021/es0486768

Rathi, B., Neidhardt, H., Berg, M., Siade, A., & Prommer, H. (2017). Processes governing arsenic retardation on Pleistocene sediments: Adsorption experiments and model-based analysis. *Water Resources Research*, *53*, 4344–4360. https://doi.org/10.1002/2017WR020551

Raven, K. P., Jain, A., & Loeppert, R. H. (1998). Arsenite and arsenate adsorption on ferrihydrite: Kinetics, equilibrium, and adsorption envelopes. *Environmental Science & Technology*, *32*(3), 344–349. https://doi.org/10.1021/es970421p

Rawson, J., Prommer, H., Siade, A., Carr, J., Berg, M., Davis, J. A., & Fendorf, S. (2016). Numerical modeling of arsenic mobility during reductive iron-mineral transformations. *Environmental Science & Technology*. https://doi.org/10.1021/acs.est.5b05956

Rawson, J., Siade, A., Sun, J., Neidhardt, H., Berg, M., & Prommer, H. (2017). Quantifying reactive transport processes governing arsenic mobility after injection of reactive organic carbon into a Bengal Delta Aquifer. *Environmental Science & Technology*, *51*(15), 8471–8480. https://doi.org/10.1021/acs.est.7b02097

Rayment, G., & Lyons, D. J. (2011). *Soil chemical methods: Australasia (Australian soil and land survey handbook series: v.3). Australian soil and land survey handbook series*. Collingwood, VIC: CSIRO Publishing.

Schraufnagel, R. A. (1993). Coalbed methane production. In *Hydrocarbons from Coal: AAPG studies in geology* (Vol. 38, pp. 341–359).

Seibert, S., Atteia, O., Salmon, U. S., Siade, A., Douglas, G., & Prommer, H. (2016). Identification and quantification of redox and pH buffering processes in a heterogeneous, low carbonate aquifer during managed aquifer recharge. *Water Resources Research*, *52*, 4003–4025. https://doi.org/10.1002/2015WR017802

Seibert, S., Prommer, H., Siade, A., Harris, B., Trefry, M., & Martin, M. (2014). Heat and mass transport during a groundwater replenishment trial in a highly heterogeneous aquifer. *Water Resources Research*, *50*, 9463–9483. https://doi.org/10.1002/2013WR015219

Siade, A., Nishikawa, T., & Martin, P. (2015). Natural recharge estimation and uncertainty analysis of an adjudicated groundwater basin using a regional-scale flow and subsidence model (Antelope Valley, California, USA). *Hydrogeology Journal*, *23*(6), 1267–1291. https://doi.org/10.1007/s10040-015-1281-y

Smedley, P. L., & Kinniburgh, D. G. (2002). A review of the source, behaviour and distribution of arsenic in natural waters. *Applied Geochemistry*, *17*(5), 517–568. https://doi.org/10.1016/S0883-2927(02)00018-5

Sreekanth, J., & Moore, C. (2015). *CSG water injection impacts: Modelling, uncertainty and risk analysis; Groundwater flow and transport modelling and uncertainty analysis to quantify the water quantity and quality impacts of a coal seam gas produced water injection scheme in the Surat Bas*. Canberra, ACT: CSIRO.

Stachowicz, M., Hiemstra, T., & van Riemsdijk, W. H. (2006). Surface speciation of As(III) and As(V) in relation to charge distribution. *Journal of Colloid and Interface Science*, *302*(1), 62–75. https://doi.org/10.1016/j.jcis.2006.06.030

Stachowicz, M., Hiemstra, T., & van Riemsdijk, W. H. (2008). Multi-competitive interaction of As(III) and As(V) oxyanions with Ca2+, Mg2+, PO3 − 4, and CO2 − 3 ions on goethite. *Journal of Colloid and Interface Science*, *320*(2), 400–414. https://doi.org/10.1016/j.jcis.2008.01.007

Stoliker, D. L., Kent, D. B., & Zachara, J. M. (2011). Quantifying differences in the impact of variable chemistry on equilibrium Uranium(VI) adsorption properties of aquifer sediments. *Environmental Science & Technology*, *45*(20), 8733–8740. https://doi.org/10.1021/es202677v

Stollenwerk, K. (1998). Molybdate transport in a chemically complex aquifer: Field measurements compared with solute-transport model predictions. *Water Resources Research*, *34*(10), 2727–2740. https://doi.org/10.1029/98WR02163

Tartakovsky, D. M., Dentz, M., & Lichtner, P. C. (2009). Probability density functions for advective-reactive transport with uncertain reaction rates. *Water Resources Research*, *45*, W07414. https://doi.org/10.1029/2008WR007383

Thi Hoa Mai, N., Postma, D., Thi Kim Trang, P., Jessen, S., Hung Viet, P., & Larsen, F. (2014). Adsorption and desorption of arsenic to aquifer sediment on the Red River floodplain at Nam Du, Vietnam. *Geochimica et Cosmochimica Acta*, *142*, 587–600. https://doi.org/10.1016/j.gca.2014.07.014

Tonkin, M., & Doherty, J. (2009). Calibration-constrained Monte Carlo analysis of highly parameterized models using subspace techniques. *Water Resources Research*, *45*, W00B10. https://doi.org/10.1029/2007WR006678

Vanderzalm, J. L., Dillon, P. J., Barry, K. E., Miotlinski, K., Kirby, J. K., & La Salle, C. L. (2011). Arsenic mobility and impact on recovered water quality during aquifer storage and recovery using reclaimed water in a carbonate aquifer. *Applied Geochemistry*, *26*(12), 1946–1955. https://doi.org/10.1016/j.apgeochem.2011.06.025

Vrugt, J. A., ter Braak, C. J. F., Gupta, H. V., & Robinson, B. A. (2009). Equifinality of formal (DREAM) and informal (GLUE) Bayesian approaches in hydrologic modeling?. *Stochastic Environmental Research and Risk Assessment*, *23*(7), 1011–1026. https://doi.org/10.1007/s00477-008-0274-y

Wallis, I., Prommer, H., Pichler, T., Post, V., B. Norton, S., Annable, M. D., & Simmons, C. T. (2011). Process-based reactive transport model to quantify arsenic mobility during aquifer storage and recovery of potable water. *Environmental Science & Technology*, *45*(16), 6924–6931. https://doi.org/10.1021/es201286c

Wallis, I., Prommer, H., Simmons, C. T., Post, V., & Stuyfzand, P. J. (2010). Evaluation of conceptual and numerical models for arsenic mobilization and attenuation during managed aquifer recharge. *Environmental Science & Technology*, *44*(13), 5035–5041. https://doi.org/10.1021/es100463q

Welch, A. H., Westjohn, D. B., Helsel, D. R., & Wanty, R. B. (2000). Arsenic in ground water of the United States: Occurrence and geochemistry. *Ground Water*, *38*(4), 589–604. https://doi.org/10.1111/j.1745-6584.2000.tb00251.x

Welter, D. E., White, J. T., Hunt, R. J., Doherty, J. E., & Survey, U. S. G. (2015). *Approaches in highly parameterized inversion—PEST++ Version 3, a parameter ESTimation and uncertainty analysis software suite optimized for large environmental models. Techniques and methods*. Reston, VA. https://doi.org/10.3133/tm7C12